AN EVALUATION OF ANGULAR SETUP ERRORS IN A NEW PATIENT-ISOLATED TRANSVAGINAL CONE SYSTEM

A Thesis

Submitted to the Graduate Faculty of the
Louisiana State University and
Agricultural and Mechanical College
in partial fulfillment of the
requirements for the degree of

Master of Science

in

Nuclear Science
(Medical Radiation Science Option)

by
Mary Jeanne Haik
B.S., Louisiana State University, 1982
December 1988

TABLE OF CONTENTS

ACKNOWLEDGMENTS

I would like to express my sincere appreciation to the entire staff at Mary Bird Perkins Cancer Center who have all made my clinical work very pleasant and enlightening. I especially want to acknowledge Mr. Michael H. Martin who has provided the recourses necessary to do thorough and expeditious research. I also thank Ms. Ajaye Bloomstone whose expertise in the field of Library Science has certainly made my life "*during thesis*" much nicer as well as improving the quality of my research.

Special thanks are extended to Ms. Carrie White Rudolf who, on her own time and with much patience, shared her knowledge and experience with me; on a one-to-one basis she gave guidance, advice, instruction, and support. I must also include Dr. Oscar Hidalgo who was always eager to provide explanations when needed.

Ms. Pat Summers deserves a very special note of appreciation for the kindness and patience she extended to me week after week (in spite of her heavy workload) during our dosimetry sessions. But not only did Pat set time aside to teach me, she was always willing to help me with any questions or problems that arose.

I want to express gratitude to Dr. Robert Fields, Dr. Kenneth Lo, and Adjunct Professor of Nuclear Science, Dr. Sheldon Johnson who have, despite their very busy schedules, always made time for students and been tolerant to their inexperience and need for special attention.

I am grateful to Mr. Audrey Audoin and Mr. Jim Davis for their

willingness to help whenever possible and for lending their technical assistance when requested.

My thanks also go out to Mr. C. W. Streate who allowed me to become his shadow day in and day out for two weeks so that I could become proficient in the mold room responsibilities.

My sincere appreciation goes to Ms. Meredith Connelly who has taken it upon herself to provide me with countless journal articles and other research literature that she has "*come across*" in her work. In addition, I would like to thank Meredith for the excellent editing job she did and Dr. Sheldon Johnson for providing the funds for her work.

Had it not been for my professors of the Nuclear Science Center who devoted much of their out-of-class time answering my numerous questions, I may never have completed my required coursework. So -- to Dr. Jack Courtney, Dr. Max Scott, Dr. Ron Knaus, and of course Dr. Edward Lambremont, I give many many thanks. I must single out Dr. Max Scott who without a doubt taught me many of the basics (and I emphasize basics) which served as a good foundation upon which to build.

To Dr. Lambremont I extend my gratitude for giving this opportunity to me by allowing my admission into the program. In addition, he has proven to be a good friend (and of course a great cook) who has helped me through some very trying times during my graduate studies.

I must also acknowledge Mr. Allen Young who creatively, accurately, and expeditiously constructed the transvaginal cones and accessories utilized for this resarch.

I would like to express my appreciation to Mr. Richard Teague who

without a doubt, has more technically-related hobbies and talents than anyone I know of, and who has always been willing to share his expertise. So to Richard, thank you for your photographic and computer graphics assistance in the project -- they were greatly appreciated.

To Yvonne Thomas, a skillful, creative typist and a true friend who has provided relentless support and has been very tolerant to my quite often "*nit picky*" nature, I give a thousand, thousand thank yous.

Another very special note of appreciation goes to Mr. William S. Kubricht, Jr. who has provided guidance and support to me throughout this endeavor. He has spent hundreds of hours working with me, been rudely awakened morning and night, and missed out on numerous weekend fishing expeditions solely because of this project.

Most of all I thank my husband Jeff for his love, support, understanding, fun times, creative contributions to my thesis, and occasional calculus tutoring which have all played a major role in my apparent achievements.

Finally, I thank my parents who have believed in me from the start.

LIST OF TABLES

LIST OF FIGURES

ABSTRACT

Traditionally, transvaginal cones have been attached or "docked" to the gantry which may compromise verification of field coverage. Docked cones also create the potential for harm to the patient whenever the cone is in place, since any sudden movement of the couch or gantry could result in serious injury to the patient. Although separation of the cone from the gantry eliminates this danger, the likelihood of gantry alignment errors arises during patient setup. This study was undertaken to evaluate the effects of gantry alignment errors on the isodensity distributions and the dose at d_{max} using "non-docked" transvaginal electron cones at a fixed target-to-surface distance (TSD). The cones evaluated were of two types, one having no bevel (0^{o} bevel) while the other had a 45^{o} bevel. The study employed electron beams of 9, 12, 16, and 20 MeV produced by a Varian Clinac 20 linear accelerator. Film dosimetry was utilized with radiographic film vertically compressed between sheets of a polystyrene phantom. Isodensity curves and central axis depth-density curves were generated by an automatic isodensitometer to illustrate the effects of gantry alignment errors. An ionization chamber was placed at d_{max} in the phantom to quantify the effects of angular errors on the dose at d_{max}. Film dosimetry was further employed to measure radiation leakage and to determine cone ratios. The leakage radiation was determined to be acceptable. The cone ratios were also determined with an ionization chamber and these results were compared to those obtained with film and found to differ insignificantly. The effect

of angular errors on the isodensity distributions and on the dose at d_{max} was found to depend upon the cone diameter and upon the energy of the beam; angular errors had less of an effect when the larger cones and higher energies were employed.

INTRODUCTION

"Cancer is the second most common cause of death in women and gynecological cancers play a significant part" (ACS, 1983). Cancers of the ovary and uterus are responsible for about 10 percent of the cancer deaths in females (ACS, 1983). Cancer of the ovary, the fourth leading cause of cancer deaths in women, is responsible for more than 11,000 deaths per year in the United States (ACS, 1983). Cancer of the uterus, the most prevalent of the gynecological cancers, is responsible for 10 percent of the cancers which occur in females today.

The role of surgery has been, and continues to be, "central to the management of most gynecological neoplasia" (ACS, 1983). But with the advancement of radiation therapy technology and the enhanced knowledge of radiation biology, radiation therapy -- external beam irradiation, intracavitary irradiation, interstitial implant, and transvaginal irradiation -- is established as a supplemental modality.

Radiation treatment plans are designed individually for each patient depending upon the clincial and surgical stage of the cancer and site of the disease. External beam irradiation may assure adequate dosages to node-bearing areas (if the nodes are included in the irradiated field), while intracavitary and interstitial irradiation deliver high doses to the central tumor. Transvaginal irradiation does not treat the nodes, paracervical tissue, or deep into the uterus. However, with transvaginal irradiation, large doses can be administered directly to the tumor without traversing normal, intervening tissue, or requiring hospitalization. Transvaginal irradiation may be used as all or part of

the treatment of carcinoma of the cervical stump and vagina depending on the stage and site of the disease (Del Regato, 1965; Johnson, 1988). When treating definitively with transvaginal irradiation, conventionally a fractionated regimen is employed (Johnson, 1988). However, transvaginal irradiation is rarely used to treat definitively since it is limited by the geometry; very few tumors provide a 1 to 2 cm margin which is needed for definitive treatment. With carcinoma of the cervical stump, the absence of the uterine cavity makes intracavitary therapy less effective (Del Regato and Ackerman, 1977; Caulk, 1956). Transvaginal therapy may be effective as a boost to external beam irradiation in the treatment of carcinoma of the cervical stump, depending on the geometry.

Treatment of carcinomas in the upper one-third of the vagina may also be effectively boosted with transvaginal therapy, if the cone can be placed to cover the lesion with a 1 to 2 cm margin of normal vaginal tissue (Fletcher, 1966). In addition, transvaginal irradiation is adopted to reduce the size of exophytic lesions and to control profuse cervical hemorrhaging (Levitt and Tapley, 1984). To control bleeding, large doses, frequently 5 to 15 Gy, are delivered in 1 to 3 fractions (Johnson, 1988). Finally, transvaginal cones can be used externally as contact cones when effective positioning of the gantry cannot be attained, for example, with labial lesions.

Historical Review

As early as 1902, C. W. Allen described and used a transvaginal cone (Merrit, 1939); Furthermore, in 1902 E. W. Caldwell wrote

> "It has been noticed that the x-ray when used as a therapeutic agent, is most effective when the part under treatment is superficial or so situated that the rays can reach it directly....."

To accomplish this he contrived an apparatus which could be placed in the mouth so that the x-rays could be directed onto the larynx (Caldwell, 1902) (Figure 1). Others, including Brichner, delved into the research of transvaginal/intraoral techniques of irradiation. He used a Ferguson vaginal speculum in 1903 (Figure 1), to treat cancer of the cheek (Brickner, 1903; Del Regato, 1948). Other investigations followed but, according to Merrit, by 1920 the method of intravaginal x-ray therapy had fallen into disuse for "one reason or another," and became "the exception rather than the rule" (Merrit, 1939).

Although Merrit acknowledged the superiority of radium in treating the cavities, he was also aware that radium was still not readily available to all (1921). He saw transvaginal therapy as a possible alternative for intracavitary radium. He eventually abandoned the technique because of "hazards associated with the use of unprotected tubes and high tension leads" (Merrit, 1937). With the technological advancement of shock proof apparatus, intravaginal treatments became less dangerous to the patient and research in the field of transvaginal therapy was revived. By 1937 Dr. Merrit had become "the forceful advocate of transvaginal roentgentherapy" (Del Regato, 1948). He employed transvaginal roentgentherapy in 112 cases of carcinoma of the cervix and concluded that the results were "superior to any previous experience" (Merrit, 1939). Merrit also applied the Ferguson vaginal speculum intraorally to treat cancers of the buccal mucosa, tongue, posterior pharyngeal wall, and soft palate.

Another contribution in the historical development of transvaginal therapy is Erskine's unique expanding speculum (Figure 2). In an effort

Caldwell's tube (Caldwell, 1902) along with Pennington's metallic shield and animal tissue cot (Pennington, 1909).

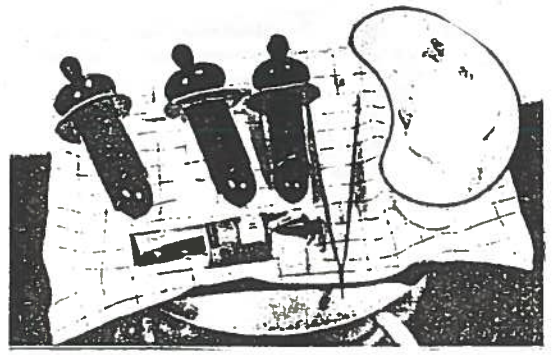

Ferguson's Bakelite specula equipped with obturators to facilitate insertion (Merrit, 1939).

Merrit's glass specula (made from urine specimen bottles accompanied by the rubber ball (to facilitate insertion) and metal cone (Merrit, 1921).

Figure 1. Transvaginal Cones of the Past

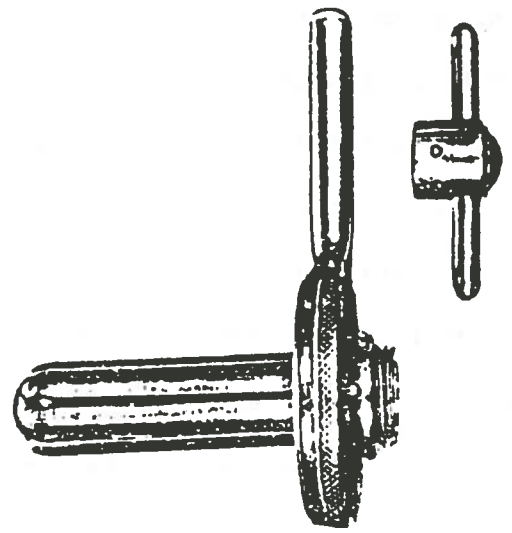

Figure 2.1

Erskine's expanding speculum with the blades closed. In an effort to increase the amount of area treated without over-irradiating the vulva and vagina, Erskine devised an expanding speculum which would retract the vaginal wall.

Figure 2.2

Erskine's speculum with the blades expanded (Erskine, 1939).

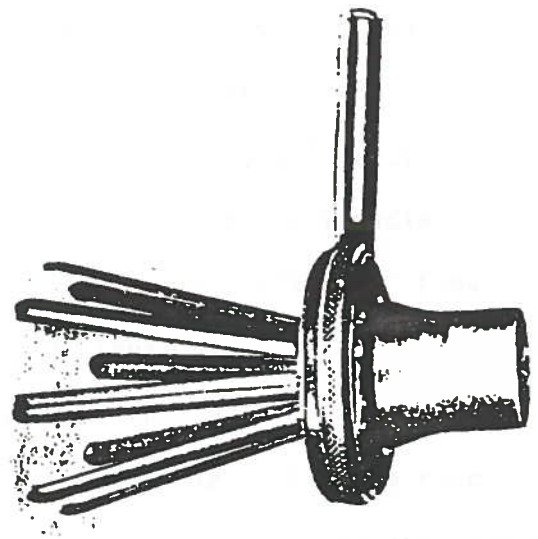

varied. But until 1976 only kilovoltage x-rays (125-220 kv) had been utilized in transvaginal irradiation. In 1976 electron beams of 6, 9, 12, 15, and 18 MeV were used with intraoral cones on a Varian Clinac-18 linac (Bigg, et al., 1982). McGinnes and Bischof also in 1976, described "intracavitary applicators adapted from orthovoltage units for use with the Clinac 18" (Wilson, et al., 1986).

Further research in the field of transvaginal therapy resulted in modifications for improved utility and safety of these endocavitary cones. Recent modifications include the addition of viewing optics, an electromagnetic attachment device, and safety features.

Viewing optics which allowed the field to be verified and monitored continuously during the treatment were incorporated in 1983 (Swindell, 1983). Another modification, an electromagnetic clamp was incorporated (by Swindell) so that the x-ray tube housing could be abutted to the cone and rigid attachment obtained by energizing the magnet (Swindell, 1983). According to Swindell, this eliminated manipulations which could lead to misalignment.

Since these cone applicator systems are attached to the gantry, any uncontrolled movement of the couch or gantry while the cone is positioned could result in injury to the patient. Cognizant of this potential for patient injury, Biggs, et. al., (1984) contrived a breakaway safety feature for an intraoral cone system, enabling the cone "to separate from its holder if subjected to sufficent upward force."

To preclude the need for a safety feature, one might consider devising a "non-docked" transvaginal cone system. This could create a plethora of problems, including the task of designing and constructing a

alignment errors which can be tolerated may be established in developing a "non-docked" system. The investigation entailed the use of a variety of Lucite cones with four electron energies produced by a Varian Clinac 20 linear accelerator.

Film dosimetry was utilized with radiographic film vertically compressed between sheets of a polystyrene phantom. Initially, a masonite phantom was employed, but due to technical problems, the investigation was completed with the polystyrene phantom after data was obtained and documented to support this change. Isodensity curves and central axis depth-density curves were generated from the film, by an automatic isodensitometer to illustrate the effects of angular errors. Central axis depth-density curves were also generated with a MacBeth manual densitometer to determine d_{max} for each energy for the selected cones. A calibrated ionization chamber was placed at d_{max} in the phantom to quantify the effects of gantry alignment errors on the dose at d_{max}. Film dosimetry was further employed to test the cones for leakage outside of the treatment field and at the air gap between the manufacturer's conventional cone (an integral part of the system) and the transvaginal cone shield. Cone ratios were determined through film dosimetry and ionization chamber measurements, and the results obtained by the two methods were compared.

stable, easy to assemble support system for the cone and anything needed to accompany it such as a shield or final collimating device. In addition, separation of the cone from the gantry would create the likelihood of gantry alignment errors during patient setup. The incorporation of sophisticated equipment such as a laser alignment system would make alignment errors improbable. However, one should not assume that such an addition is justified since neither the effect, nor the probability of such errors has been investigated.

At the St. Bartholomew Hospital's 50th Anniversary Conference in London, Jones, et. al., (September, 1987) reported on a "non-contacting intracavitary electron cone apparatus." They identified the principal weaknesses of current intracavitary cone systems as "(1) nonoptimized beam characteristics resulting in gross nonuniformity in the irradiated field, and (2) the attachment of the patient to the radiotherapy machine with consequent hazard and time consuming docking process." Although they did not investigate the effects of beam alignment errors, their system includes "a specially designed, close-up camera" to document the set-up. This camera "has been attached to a plate of appropriate size which is precisely aligned with the beam's central axis" (Jones, et al., 1987).

The Research Objective

This research was undertaken to investigate the effects of gantry alignment errors on the isodensity distributions and the dose at d_{max}, using "non-docked" transvaginal electron cones at a fixed target-to-surface distance (TSD). By determining the significance of the errors, an appropriate "specification" allowing for the range of

MATERIALS AND METHODS

All measurements in this study were made with a Varian Clinac 20, a standing wave radio-frequency powered linear accelerator. The Clinac 20 is capable of producing beams of 15 MV photons, and 6, 9, 12, 16, and 20 MeV electrons with variable dose rates of 100-500 rads/min. Only the 9, 12, 16, and 20 MeV electron beams were employed in this investigation.

Description of the Cones and Attachments

The transvaginal cones are constructed of 1/8" thick Lucite tubing 20 cm in length. The cones evaluated in this study are of two types, one having no bevel (0° bevel or flat-end) while the other had a 45° bevel. In the first group cone diameters of 3.0, 3.8, 4.3, and 5.0 cm were utilized while the second group included cone diameters of 3.0 and 5.0 cm. Additional cones with 15° and 30° bevels were available but not evaluated in this study. The degree of beveling needed depends upon the slope of the surface being treated (Fraass, et. al., 1985).

An aluminum housing is attached to one end of the cone and secured with an adjustable screw. The aluminum housing slides into an aperture, 4.3 cm in diameter, centered in a 15x15 cm final collimating device which is referred to as the beam-defining collimator (Figure 3). The beam-defining collimator is constructed of 1/4 inch thick lead inlaid into 1/8 inch thick aluminum. Cross hairs are accurately inscribed onto the beam-defining collimator to assist in alignment during setup (Figure 4).

The standard 10x10 cm fiberglass and aluminum electron cone applicator, provided with the Varian Clinac 20, was used with the transvaginal cones throughout this study. The 10x10 cm insert was used

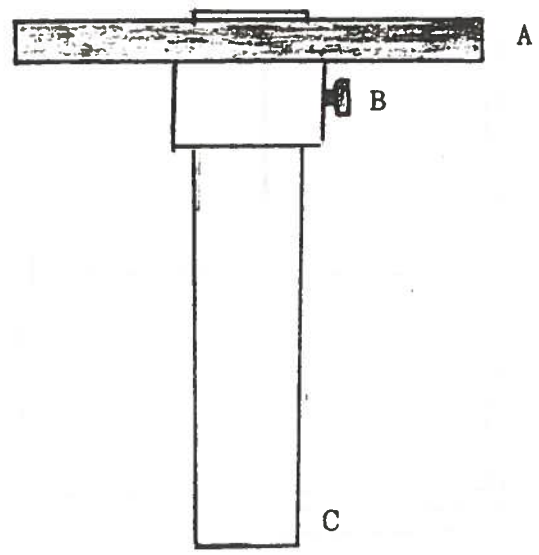

A) Beam-defining collimator

B) Aluminum housing

C) Lucite cone, 0° bevel

Figure 3. The Cone Assembly

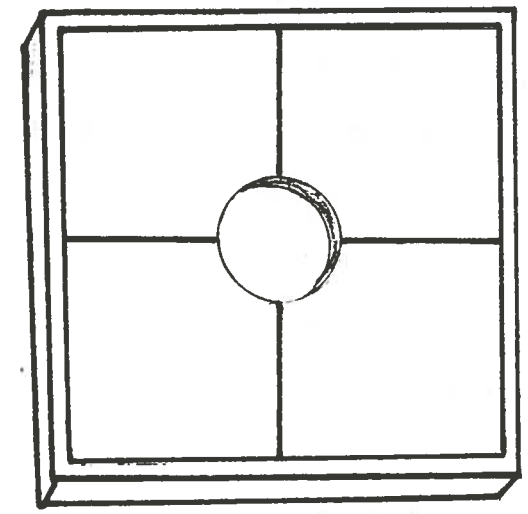

Figure 4. The Beam-Defining Collimator with the Cross Hairs Inscribed onto the Lead

with the conventional electron applicator to shape the treatment field.

Dose Response Curve

Standard dose response curves (sensitometric curves) for the 9, 12, 16, and 20 MeV electron beams were obtained using Kodak XV-2 film (Batch #122 135 and #122 131). A leveled polystyrene phantom was placed in calibration conditions: 10x10 cm field size at 100 cm target-to-phantom (TPD). Individual pieces of film were placed at d_{max} (for each energy) within the phantom. Each piece of film was given a set amount of monitor units ranging from 0-60 monitor units (MU). An unexposed piece of film was set aside for base fog subtraction, and all film was developed simultaneously the same day of exposure using the Kodak X-OMAT rapid processor. A MacBeth TD-504 densitometer was employed to obtain net optical density readings from the processed film. Optical density readings were read from the center of the radiation field for each dose delivered. From these readings, a sensitometric curve (for each batch of film) was prepared for each electron energy used in the study (Figure 5).

Before the optical density readings were obtained, calibration of the densitometer was performed using the Kodak Calibration Step Tablet (No. 706 ST121). Since the TD-504 densitometer is manually operated and calibrated, periodic calibration checks must be performed to insure that the instrument is operating accurately. This calibration check was performed before each use and if necessary the potentiometer was adjusted until the digital display corresponded to the density value assigned to each area of the calibration step tablet. This calibration allowed the direct reading of optical density with the densitometer.

with the conventional electron applicator to shape the treatment field.

Dose Response Curve

Standard dose response curves (sensitometric curves) for the 9, 12, 16, and 20 MeV electron beams were obtained using Kodak XV-2 film (Batch #122 135 and #122 131). A leveled polystyrene phantom was placed in calibration conditions: 10x10 cm field size at 100 cm target-to-phantom (TPD). Individual pieces of film were placed at d_{max} (for each energy) within the phantom. Each piece of film was given a set amount of monitor units ranging from 0-60 monitor units (MU). An unexposed piece of film was set aside for base fog subtraction, and all film was developed simultaneously the same day of exposure using the Kodak X-OMAT rapid processor. A MacBeth TD-504 densitometer was employed to obtain net optical density readings from the processed film. Optical density readings were read from the center of the radiation field for each dose delivered. From these readings, a sensitometric curve (for each batch of film) was prepared for each electron energy used in the study (Figure 5).

Before the optical density readings were obtained, calibration of the densitometer was performed using the Kodak Calibration Step Tablet (No. 706 ST121). Since the TD-504 densitometer is manually operated and calibrated, periodic calibration checks must be performed to insure that the instrument is operating accurately. This calibration check was performed before each use and if necessary the potentiometer was adjusted until the digital display corresponded to the density value assigned to each area of the calibration step tablet. This calibration allowed the direct reading of optical density with the densitometer.

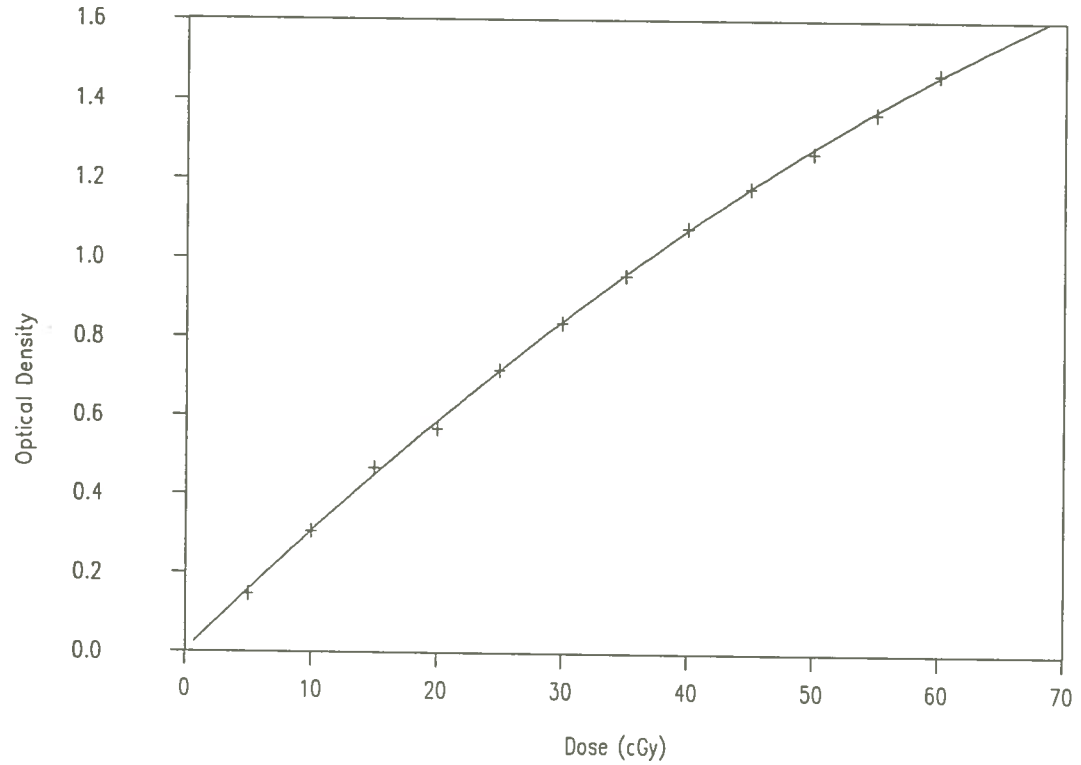

Figure 5.1 Sensitometric curve for XV-2 film exposed under calibration conditions with 9 MeV electrons.

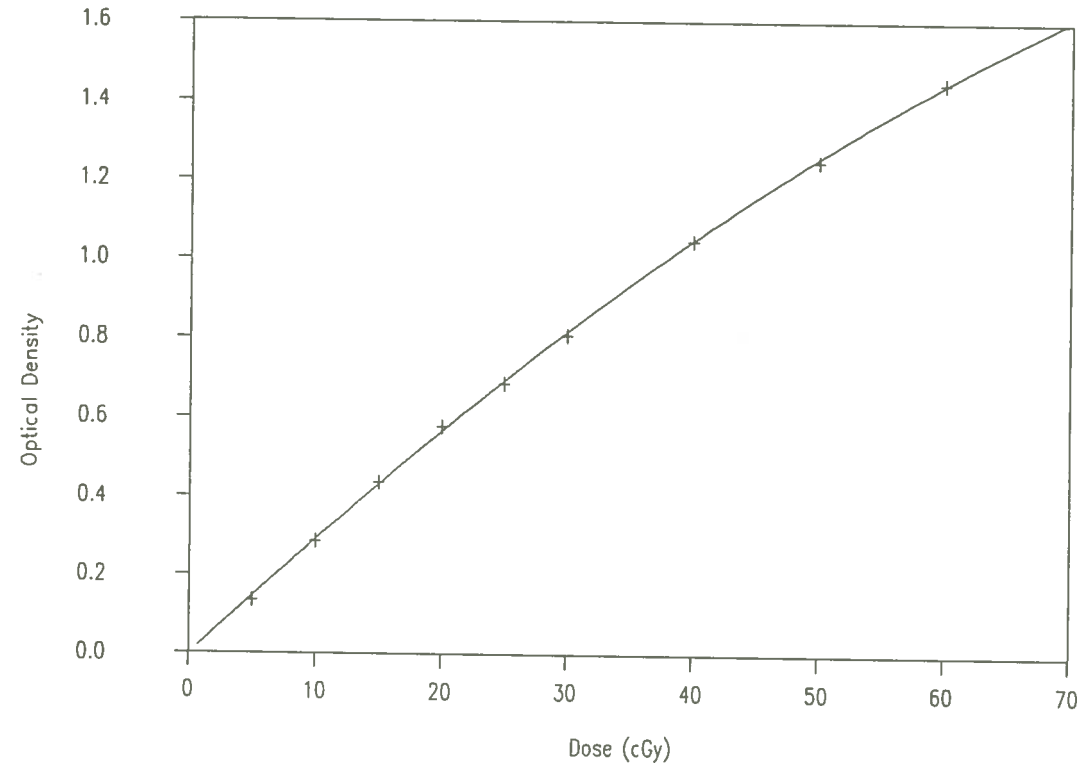

Figure 5.2 Sensitometric curve for XV-2 film exposed under calibration conditions with 12 MeV electrons.

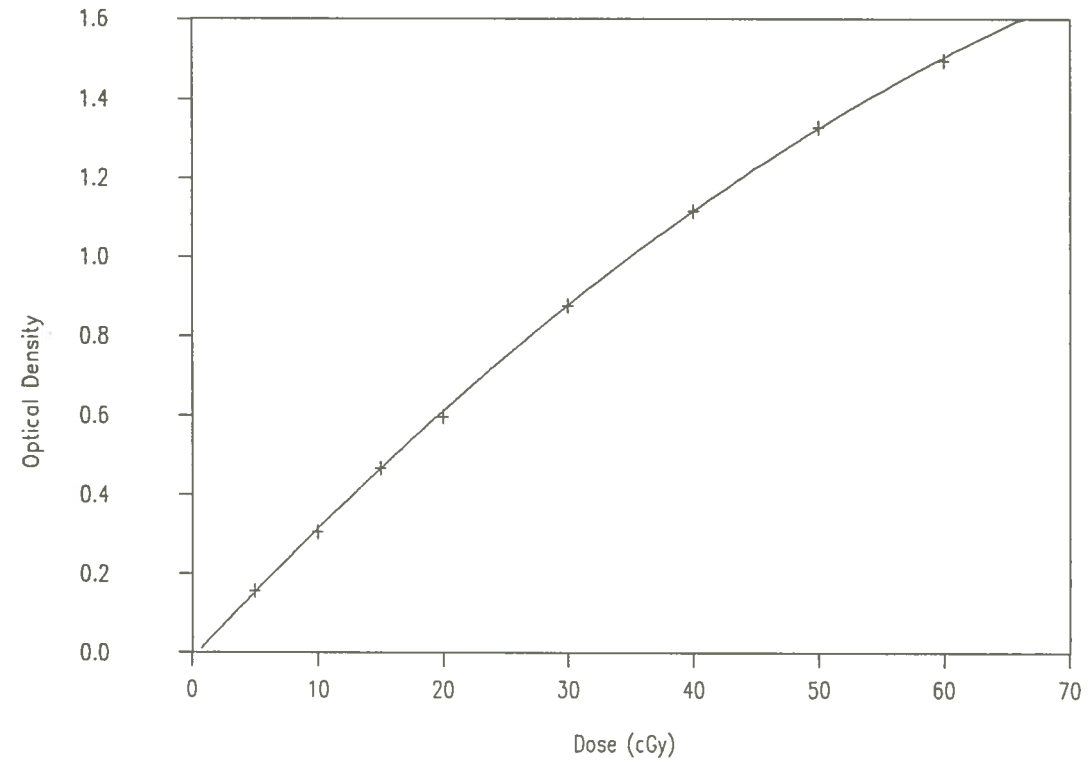

Figure 5.3 Sensitometric curve for XV-2 film exposed under calibration conditions with 16 MeV electrons.

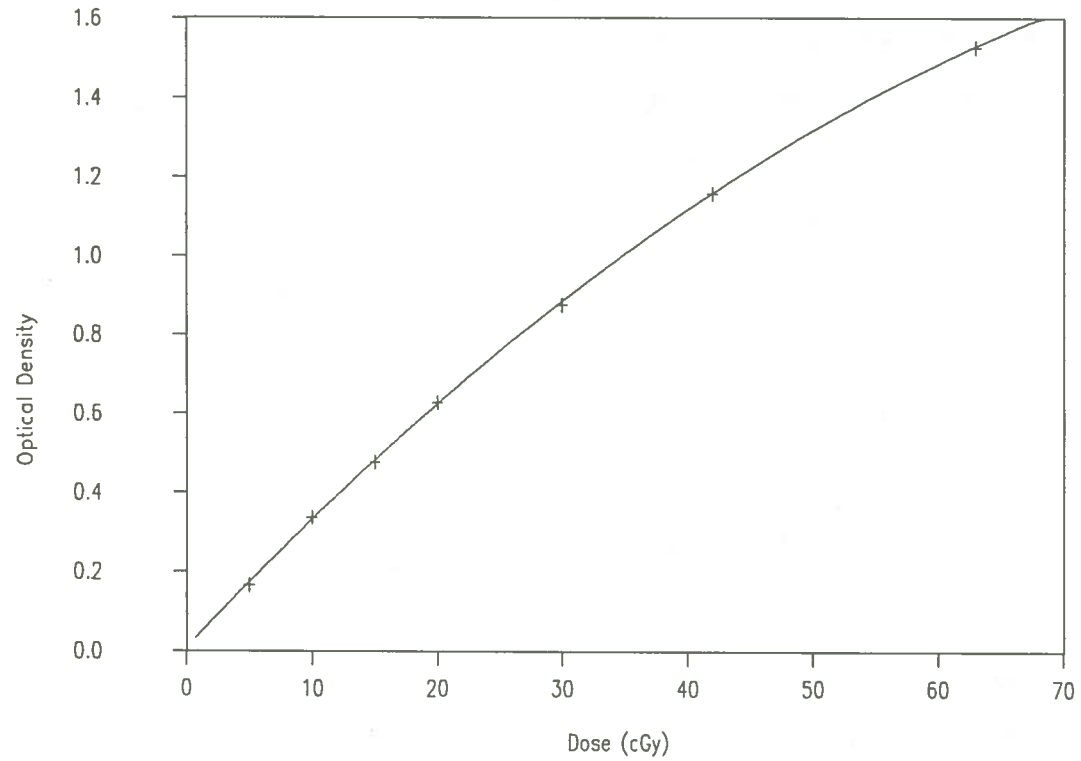

Figure 5.4 Sensitometric curve for XV-2 film exposed under calibration conditions with 20 MeV electrons.

Demonstrating the Effect of Gantry Angle Errors on Isodensity Distributions

Kodak XV-2 radiographic film (Batch #122 135 and #122 131) cut to the appropriate size was vertically compressed (in the transverse plane) between 6 mm sheets of a polystyrene phantom (26.5 x 27.5 x 30 cm, density 1.04 g/cc). Before each film exposure, the phantom was leveled with a tripod leveling pad. (Initially, the film was compressed in a masonite phantom [30x55x38 cm]. Unfortunately, the size and weight of the masonite phantom created technical problems which led to the use of the polystyrene phantom for the duration of the experiment. To support the change in phantoms, an experiment was conducted to compare the two, which is outlined in the section Comparing the Masonite and Polystyrene Phantoms.)

Because the film was positioned parallel to the beam axis, two precautions were taken to decrease the incidence and severity of errors: (1) heavy pressure was exerted on the phantom to avoid any air gaps on either side of the film. Holes were punched in the corners of the film to facilitate the escape of air when compressed; (2) care was taken to assure correct alignment of the film edge with the surface of beam entry (Dutreix and Dutreix, 1969).

The film was placed in a plane containing the beam axis in order to produce a complete set of isodensity and central axis depth-density curves on a single film (Dutreix and Dutreix, 1969, Hogstrom). Alignment of the film with the beam axis was accomplished by aligning the edge of the film with the transverse cross hair projected from the gantry (with the gantry vertical).

Accurate alignment of the non-beveled cones was accomplished

relatively easily. They were simply positioned, beam-defining collimator up, on top of the phantom. The phantom was raised to 100 cm TSD (surface of the beam-defining collimator) producing a 5cm air gap between the conventional cone and the beam-defining collimator. The gantry was leveled vertically (using a precision level) and this gantry position was taken to be perfectly vertical and recorded (though not reading 180°). The cross hairs projected from the gantry were aligned with the cross hairs on the beam-defining collimator (Figure 6).

The beveled cones, when placed on top of the phantom, required a support device to maintain each cone in a reproducible position (Figure 7). The material selected for fabrication of this device was a high density, closed cell styrofoam. The integrity of the material used for this purpose was evaluated by disassembling and reassembling the device multiple times, checking the angulation of the beam-defining collimator with a protractor.

Once the beveled cone was supported on top of the phantom, the gantry was vertically leveled and the digital readout recorded. The gantry was then angled 45 degrees off the vertical. The light field produced at the surface of the phantom was used to make fine adjustments of the gantry alignment in the x and y plane, prior to setting the 100 cm TSD (Figure 8). The distance at each of the four corners between the beam-defining collimator and the conventional cone measured 5 cm when alignment was achieved. This gantry digital readout was recorded as the angle of accurate alignment or the "assumed accurate position."

The gantry alignment errors were produced using the gantry digital indicator to vary the angle of the gantry. Initially, gantry angle

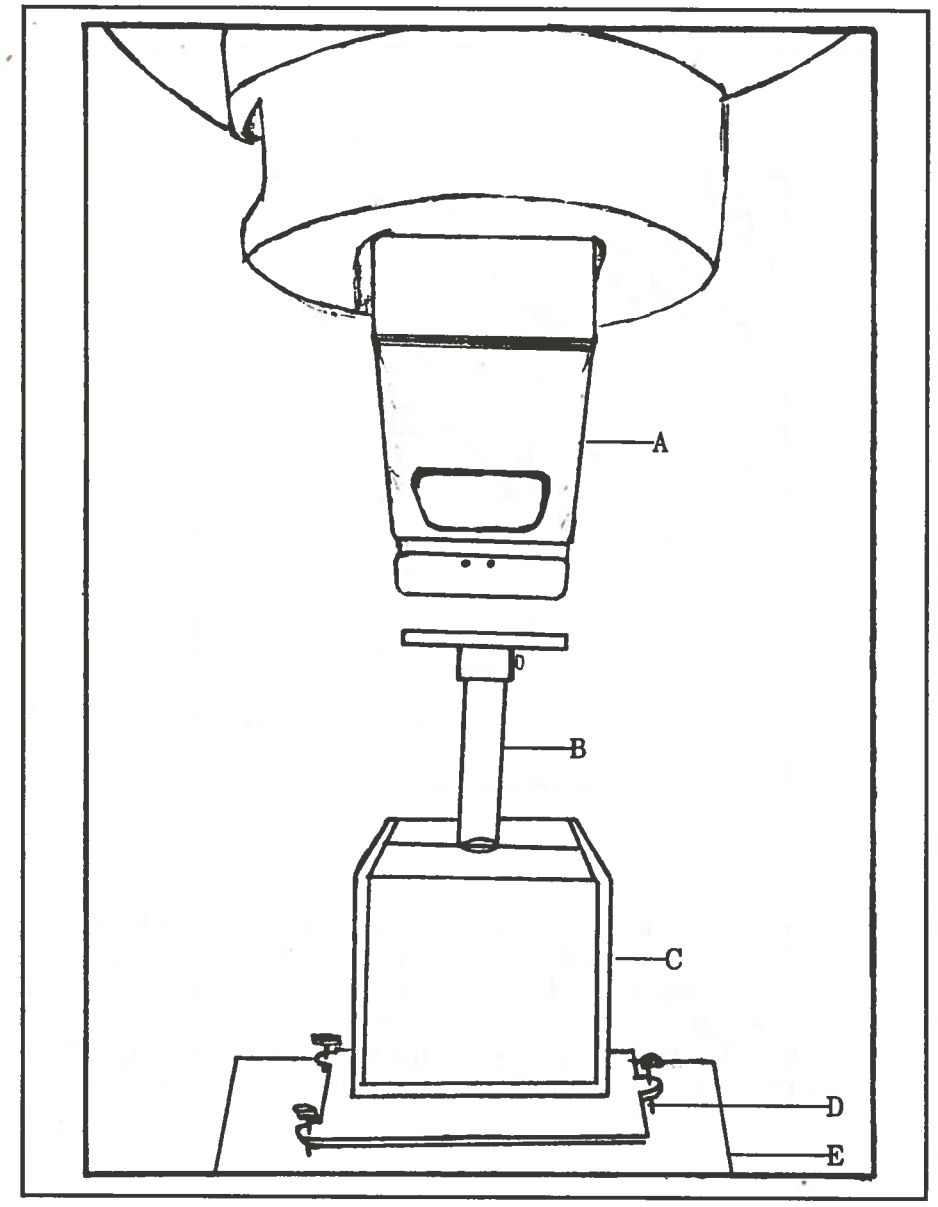

A) 10x10 conventional cone
B) transvaginal cone
C) polystyrene phantom
D) levelling pad
E) couch

Figure 6. Experimental setup for the non-beveled cones. The non-beveled cones were positioned, beam-defining collimator up, on top of the phantom. The phantom was raised to 100 cm TSD producing a 5 cm air gap between the conventional cone and the beam-defining collimator.

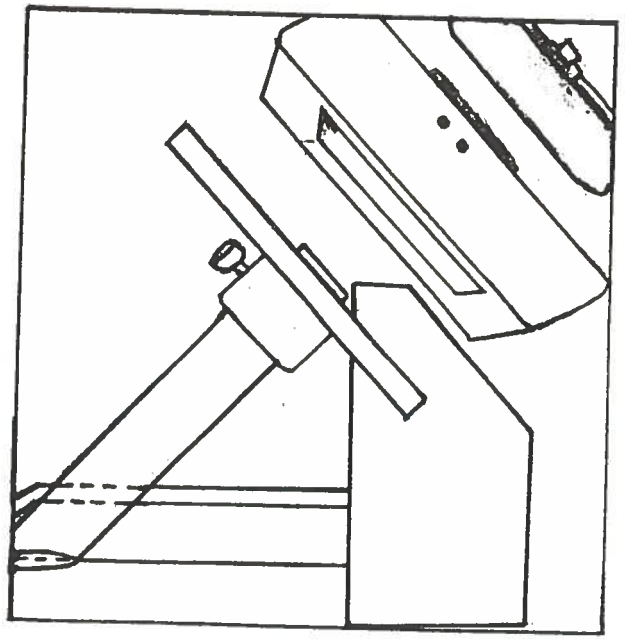

Slots of the appropriate size and angle were cut into styrofoam blocks with a heated wire. The beam-defining collimator slid into the slot for stable, reproducible support. Also, the styrofoam was cut out along the edge of the field light so that the support device did not interfere with the beam.

Figure 7. Support Device for the Beveled Cones

A) B) C)

A) Gantry tilted slightly to the left of vertical

B) Gantry tilted slightly to the right of vertical

C) Gantry approximately vertical

Figure 8. The field light produced at the surface of the phantom was used to make fine adjustments in the gantry alignment.

errors of 1, 2, 3, and 5 degrees were evaluated (with the masonite phantom) using the cone with an inside diameter of 4.3 cm and a 0° bevel. The remaining three cones (with a 0° bevel) included a 4° gantry angle error in their evaluation. Electron beams of 9, 12, 16, and 20 MeV were applied with each cone at the position assumed to be vertical and at each of the error positions.

For the beveled cones, a film was exposed at the position assumed to be accurate, and at 1, 2, 3, 4, and 5 degrees plus this position. In addition, with the 9 and 20 MeV electron beams, films were also irradiated at the "assumed accurate postion" minus 1, 2, 3, 4, and 5 degrees in order to determine how errors made in opposite directions might differ (Figure 9).

For the 9 MeV electron beam, 85 monitor units (MU) were delivered while only 75 MU were delivered for the 12, 16, and 20 MeV electron beams. Although it was not the intent of this thesis to convert net optical density (obtained from the film) to dose, the monitor units were adjusted so that the optical density readings obtained would fall on the linear portion of the dose response curve. (See section on Dose-Response Curve for details.)

The exposed films were developed simultaneously by a Kodak X-OMAT rapid processor on the day of exposure in order to increase the accuracy of data obtained from the films (Dutreix and Dutreix, 1959). The films were then read by an Artronix automatic isodensitometer (Model 1705), renormalized to a net optical density of zero before each use, to generate isodensity curves and central axis depth-density curves.

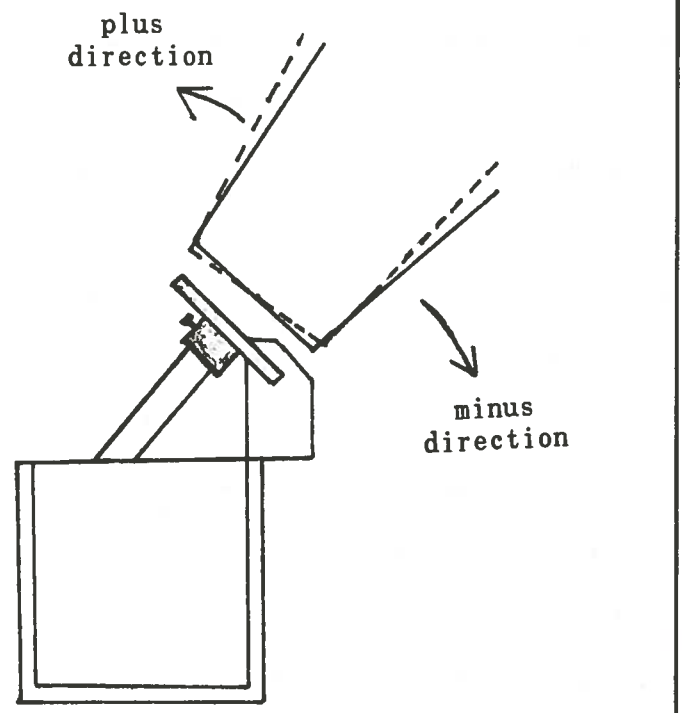

Figure 9. Angular errors in the minus and plus directions. When the beveled cones were employed, angular errors in both directions were evaluated, in order to determine how errors made in opposite directions might differ in their effect.

Comparing the Masonite and Polystyrene Phantoms

Initially, in demonstrating the effect of gantry angle errors with film, the film was vertically compressed in the leveled masonite phantom. The non-beveled cone with an inside diameter of 4.3 cm was used to irradiate the film with 9, 12, 16, and 20 MeV electron beams, with the gantry accurately and inaccurately aligned, under the conditions described in the previous section. Data extracted from the film exposed (in the masonite phantom) with accurate gantry alignment were used in this comparison.

The same transvaginal cone (4.3 cm 0° bevel) was employed with each of the same four electron beams to irradiate film vertically compressed in the leveled polystyrene phantom. The setup conditions (i.e., TSD, etc.) were the same as previously described. The same precautions were taken in the: (1) placement of the film in the phantom, in a plane containing the beam axis, and (2) alignment of the gantry and cone.

A piece of film was exposed in each phantom, by each of the four electron energies, with the gantry accurately aligned, using the cone already specified. An unexposed piece of film was set aside for base fog subtraction. Again, the films were processed simultaneously using a Kodak X-OMAT automatic rapid processor. The films were scanned along the central axis with a MacBeth TD-504 densitometer. Net optical density readings were obtained every 2-5 mm, depending on the region of the curve, using a 1 mm reading-area insert.

The net optical density readings obtained were used to prepare central axis depth-density curves. Data extracted from these curves provided a basis for comparing the two phantoms (Table 2 in Results Section).

Demonstrating the Effects of Gantry Alignment Errors Quantitatively

This investigation utilized a Modified Farmer-Type .2 cc volume chonka plastic cylindrical ion chamber (Model 2505/3). One hundred MU were delivered and measurements were made with a Keithley Model 616 Digital Electrometer used in conjunction with a Keithley Model 6169 ion chamber interface. The setup parameters for the electrometer were as follows: -300 V applied to the thimble of the chamber, 3/5 sensitivity, 10^{-8} Coulombs, fast mode. The leakage current measured and recorded was negligible (2×10^{-14} A).

The ion chamber was placed at d_{max} in a polystyrene phantom which was leveled with a tripod leveling pad. The values for d_{max} (for each energy) were determined from the central axis depth-density curves for each cone. These curves were generated from films previously exposed with the gantry accurately aligned. The values for d_{max} obtained from the curves were adjusted with a displacement correction factor.

It has been demonstrated experimentally that the effective point of measurement for an electron beam is displaced from the center of the ion chamber toward the source of the beam: "The displacement of the effective point of measurement is about 0.45r for 3-10 MeV electrons and 0.6r for 10-30 MeV electrons, where r is the radius of the chamber" (Khan, 1984). This correction was applied and the appropriate amount of buildup was added so that the chamber was situated at d_{max}.

For the non-beveled cones, the gantry was leveled vertically and the digital readout was recorded as the accurate gantry angle. The gantry cross hairs were aligned with the cross hairs marked on the phantom, thus placing the beam axis at the center of the sensitive volume of the chamber. The cones were placed on the phantom and it was raised to 100

cm TSD. The cross hairs on the beam-defining collimator were aligned with the gantry cross hairs so that the central axis of the beam passed through the center of the cone. Accurate alignment of the non-beveled cones was once again relatively simple.

On the other hand, accurate alignment of the beveled cones was complex and tedious. Aligning the beam axis with the center of the ion chamber required shifting the radial cross hair on the phantom, a distance equal to c•Cos θ (Figure 10). By shifting the cross hair, the central axis of the beam, although entering the phantom at approximately a 45° angle, was centered on the sensitive volume of the chamber. Next, the cone, supported by the styrofoam support described earlier, was placed on top of the phantom. The accurate gantry angle was achieved by the same procedure already discussed, and the target-to-shield distance remained 100 cm. Finally, the gantry cross hairs were carefully aligned with the modified cross hairs on the phantom, as well as with those on the beam-defining collimator.

After proper alignment was achieved, three readings at each data point were taken, using each cone and each energy. Throughout the study, each data point comprised three readings which were averaged.

For the cones with no bevels, measurements were taken at 1, 2, 3, and 5 degrees error. Additional gantry angle errors were investigated in the evaluation of the beveled cones. When the 9 and 20 MeV electron beams were applied with the two beveled cones, readings were obtained at the accurately aligned position, at plus 1, 2, 3, 4, and 5 degrees, and at minus 1, 2, 3, 4, and 5 degrees (Figure 8). But data was not collected at the error positions in the minus direction when the 12 and 16 MeV beams were applied.

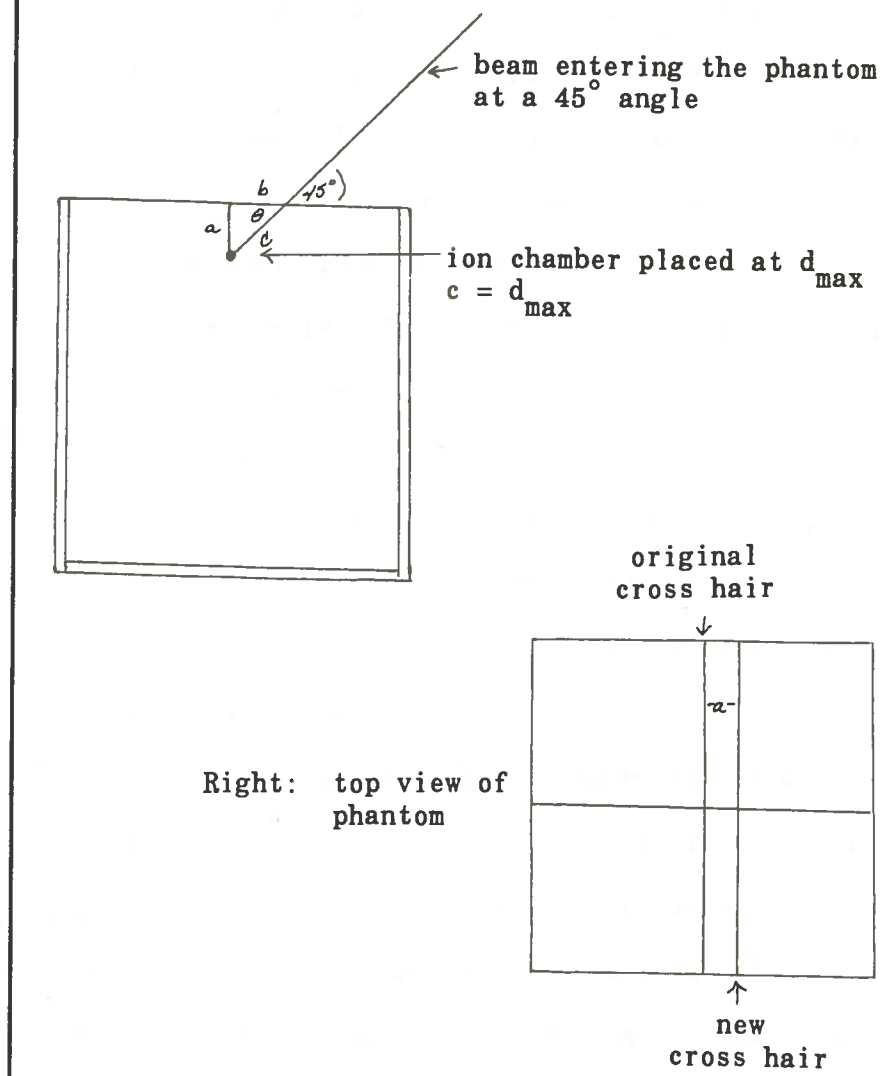

Figure 10. Shifting the radial cross hair. The radial cross hair was shifted "a" number of cm. "a" was calculated as follows: the beam entered the phantom at an angle of 45°, thus $\theta = 45°$.

Therefore a=b and $a^2+b^2=c^2$ becomes $a^2+a^2=c^2$ and $a = \sqrt{\frac{c^2}{2}}$.

Determining Cone Ratios

Cone ratios were determined by two methods (using film and an ion chamber) and the results from each method were compared. Most of the data used to determine cone ratios were obtained from previous experiments conducted: (1) to demonstrate the effects of gantry errors with film, and (2) to quantify the effects with an ion chamber.

To determine cone ratios with film, the highest readings of net optical density were obtained from each film previously irradiated with no error in the gantry angle. The non-beveled cone with an inside diameter of 4.3 cm was arbitrarily chosen as the reference cone to which the others were normalized.

The cone ratios were also determined from data obtained in the quantitative evaluation of gantry alignment errors. The average reading obtained with the gantry accurately aligned (using each cone and each energy) was normalized to the same reference cone.

In addition, cone ratios were determined using the conventional 10x10 cm cone (instead of the 4.3 cm cone) as the reference cone. (The same ion chamber, electrometer, and electrometer settings discussed in the section immediately preceeding were also used in this experiment.) The .2 cc Farmer chamber was placed in calibration conditions in the polystyrene phantom (at d_{max} for each energy, 10x10 cm field size, 100 cm TPD). One hundred MU were delivered and three readings were taken for each of the four electron beams. The average reading obtained for each cone, using each energy, was then normalized to the 10x10 cm cone.

Measuring Leakage

There have been several recent investigations concerning the amount

of scatter and leakage radiations through electron beam applicators (Schneider, 1982; Keys, et. al., 1984). Leakage radiation is usually investigated to determine the dose (imparted by the leakage) to the contralateral breast or the lens of the eye (Keys, et. al., 1984). With transvaginal cones, the amount of leakage may not be as critical since the legs (instead of the eyes) are most likely to be affected. However, the subject still deserves investigation.

In this study, film dosimetry was utilized to measure the leakage. Pieces of film (Kodak XV-2 Batch #122 131) were placed in the air gap between the 10x10 cm cone and the beam-defining collimator. In addition, a piece of film was wrapped and secured around each cone with each electron energy used (Figure 11).

The largest and the smallest non-beveled cones (3.0 cm and 5.0 cm) were employed. The cones were placed on top of the leveled polystyrene phantom with the TSD remaining 100 cm. The gantry was leveled vertically and the cross hairs aligned as described previously. One hundred MU were delivered with 9, 12, 16 and 20 MeV electron beams.

The irradiated pieces of film (and one unexposed piece for background subtraction) were processed as previously described and the MacBeth densitometer was employed to obtained the net optical density readings. These readings were taken at regular intervals on each piece of film and recorded in the same pattern as they were obtained. The net optical density readings were converted to dose using the sensitometric curves prepared for each electron energy.

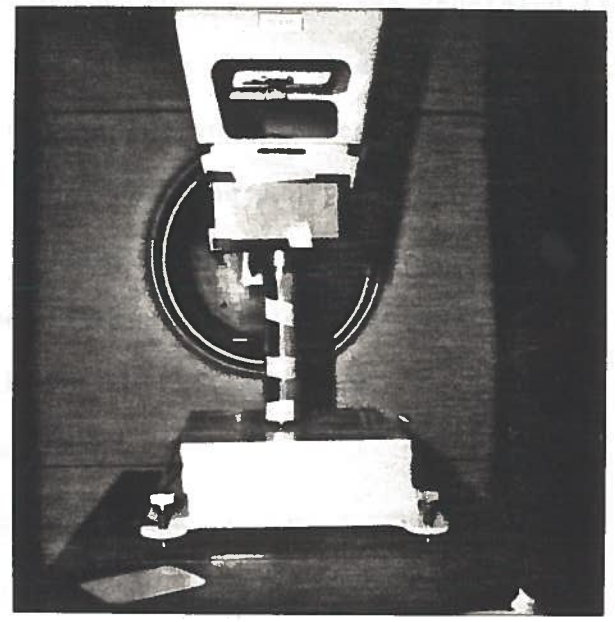

Figure 11. Setup used to measure leakage with film. Film was placed at the 5cm air gap (on all 4 sides) between the 10x10 cone and the beam-defining collimator. The sides were designated as position No. 1, 2, 3, or 4. This photo was taken facing position No. 4. Position No. 1 is to the left, position No. 2 is behind position No. 4, and position No. 3 is to the right.

RESULTS AND DISCUSSION

Dose Response Curve

All optical density data obtained in this study fell on the linear portion of each sensitometric curve (Figure 5). Therefore, small variations in dose correlated with small variations in optical density.

A central axis depth-density curve was generated from a film (compressed in the polystyrene phantom) exposed with 12 MeV electrons using the 4.3 cm non-beveled cone. Percentage of optical density versus depth was plotted. Then from the sensitometric curve prepared with 12 MeV electrons, net optical density was converted to dose, and percent dose versus depth was then plotted (Figure 12). Data obtained from these two graphs verified the correlation between optical density and dose, and are presented in Table 1.

Demonstrating the Effect of Angular Errors with Film

Through experimentation, film dosimetry has proven to be an excellent practical method (Ehrlich, 1954; Granke et al., 1954; Dudley, 1956), especially for high energy electrons (Dutreix and Dutreix, 1969). Although film dosimetry should not be used to assess absorbed dose, in relative dosimetry its reliability is satisfactory and its accuracy rivals that of other methods (Johns and Cunningham, 1983; Hogstrom; Khan, 1984).

In an attempt to eliminate errors such as those depicted in Figure 13 (Loevinger et al., 1961), precautions were taken to properly align the film with the phantom surface and to remove air gaps. In spite of these attempts to maintain a strict quality assurance, errors caused by trapped air did occur. Figure 14 provides an example of one of these errors.

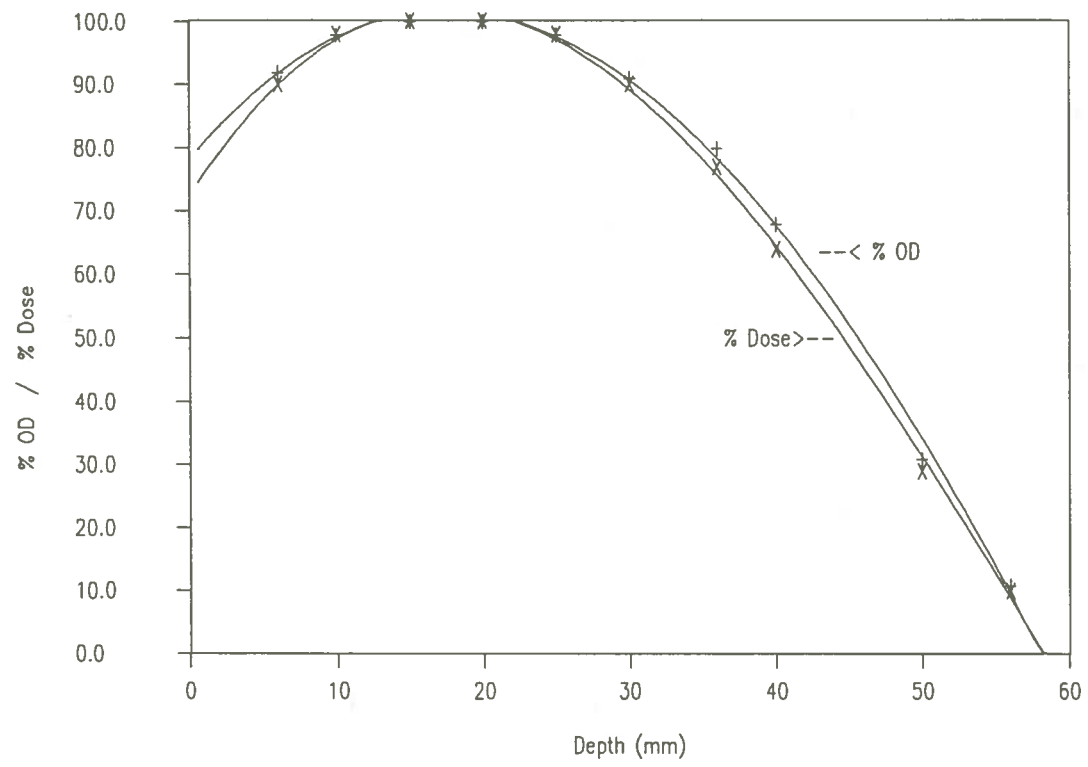

Figure 12. Curves illustrating the correlation between optical density and dose. A central axis-depth-density curve was generated from a film (compressed in the polystyrene phantom) exposed with 12 MeV electrons using the 4.3 cm non-beveled cone. Percentage of optical density versus depth was plotted. Then, using the sensitometric curve for 12 MeV electrons, net optical density was converted to dose and percent dose versus depth was plotted.

Table 1

Percent Optical Density Versus Percent Dose(*)

Depth (mm)	Net O.D.(**)	Dose (cGy)(***)	% O.D.	% Dose
6	1.07	41	92	90
10	1.14	44.5	98	98
15	1.16	45.5	100	100
20	1.16	45.5	100	100
25	1.14	44.5	98	98
30	1.06	41	91	90
36	0.93	35	80	77
40	0.79	29	68	64
50	0.36	13	31	29
56	0.13	4.5	11	10

(*) These data were obtained from the two graphs presented in Figure 12 which illustrates the correlation between optical density and dose.

(**) Net optical density, i.e., base fog, has already been subtracted. These data were obtained from the central axis depth-density curve generated from film exposed with 12 MeV electrons using the 4.3 cm non-beveled cone. Percentage of optical density versus depth was plotted from this depth-density curve (Figure 12).

(***) Using the sensitometric curve for 12 MeV electrons, net optical density was converted to dose, and percent dose versus depth was plotted (Figure 12).

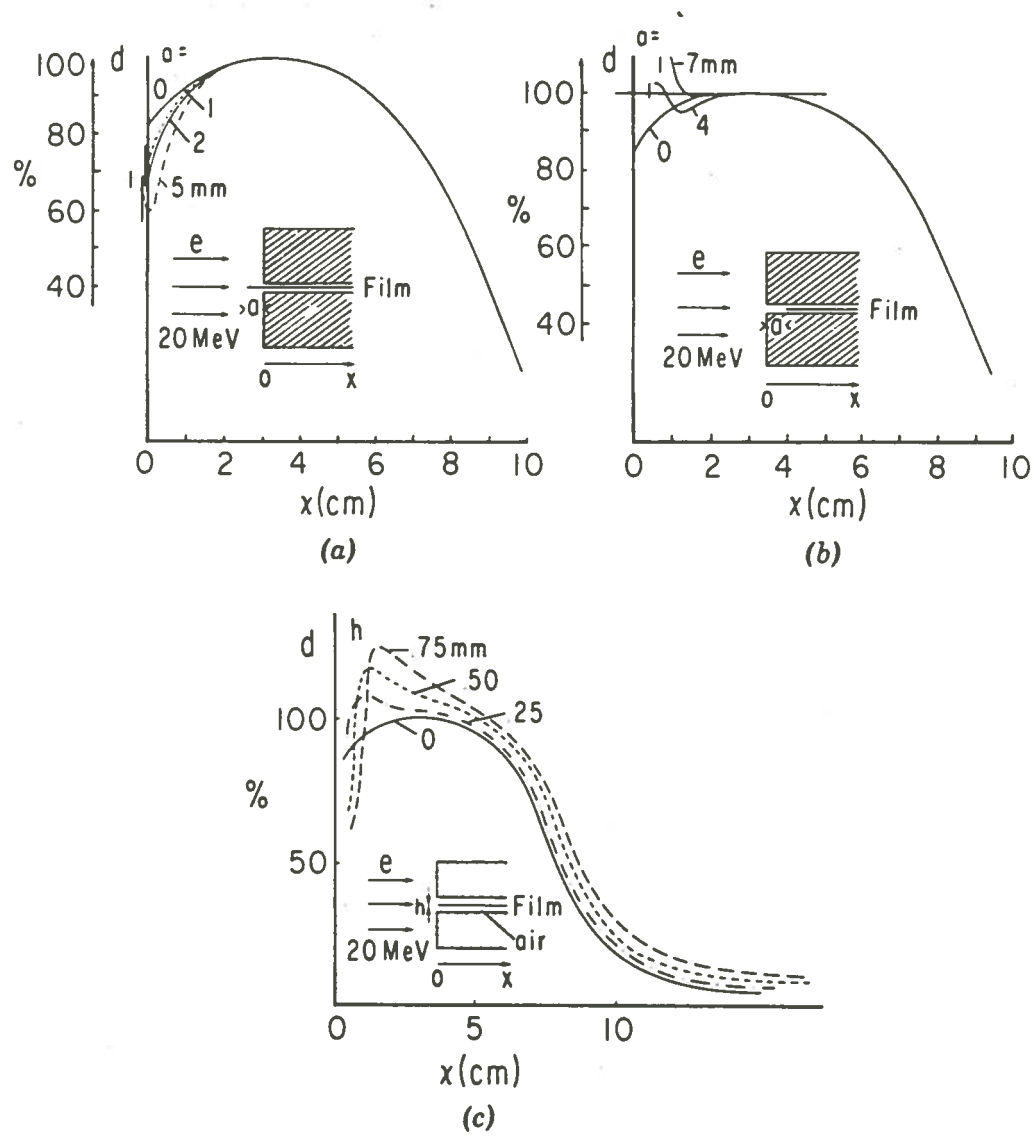

Figure 13. Influence on the depth-density curves of misalignment of the film in the phantom. Three effects can be observed: (a) if the film extends beyond the phantom, (b) if it is recessed within the phantom, and if (c) there is any air trapped between the film and the phantom (Loevinger, et al., 1961; Tapley, 1976).

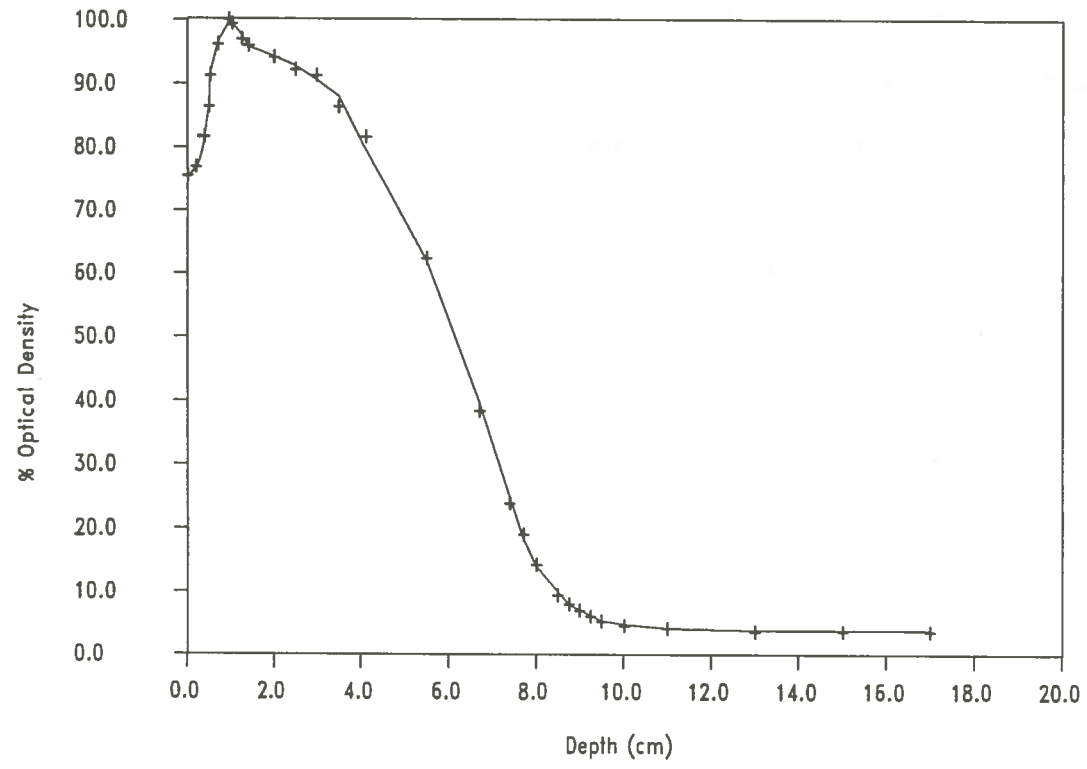

Figure 14. Depth-density curve depicting an error caused by air trapped between the film and the phantom. This curve was generated from film irradiated with 16 MeV electrons, using the 5.0 cm non-beveled cone with the gantry vertical.

Figure 15.1 Isodensity curves which demonstrate that angular errors as small as 1 or 2 degrees had greater effects on the distributions when the smaller cones were employed.

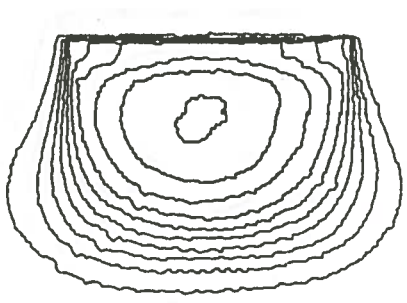

gantry vertical

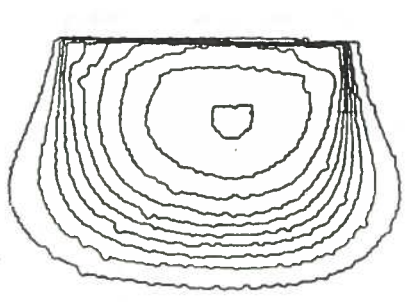

1° gantry error

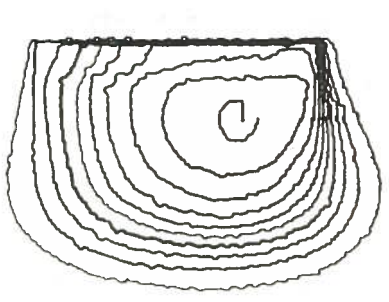

2° gantry error

Isodensity curves generated from film exposed with 9 MeV electrons utilizing the 5.0 cm non-beveled cone (above) and the 3.0 cm non-beveled cone (below). (Magnification factor for all isodensity curves presented equals 0.75).

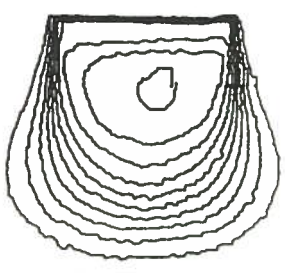

gantry vertical

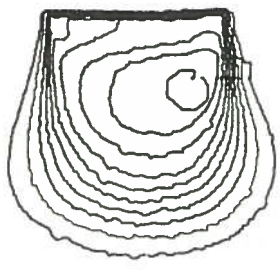

1° gantry error

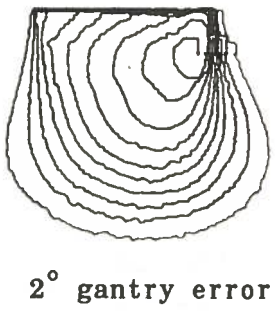

2° gantry error

Figure 15.2 Additional isodensity curves which demonstrate that the effect of angular errors depended upon cone diameter.

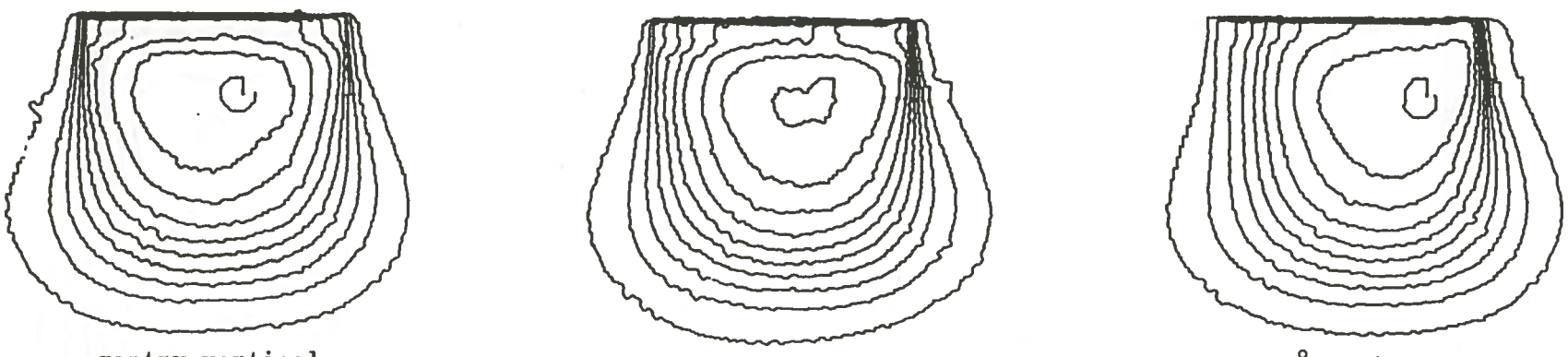

gantry vertical

1° gantry error

2° gantry error

Isodensity curves generated from film exposed with 12 MeV electrons utilizing the 5.0 cm non-beveled cone (above) and the 3.0 cm non-beveled cone (below).

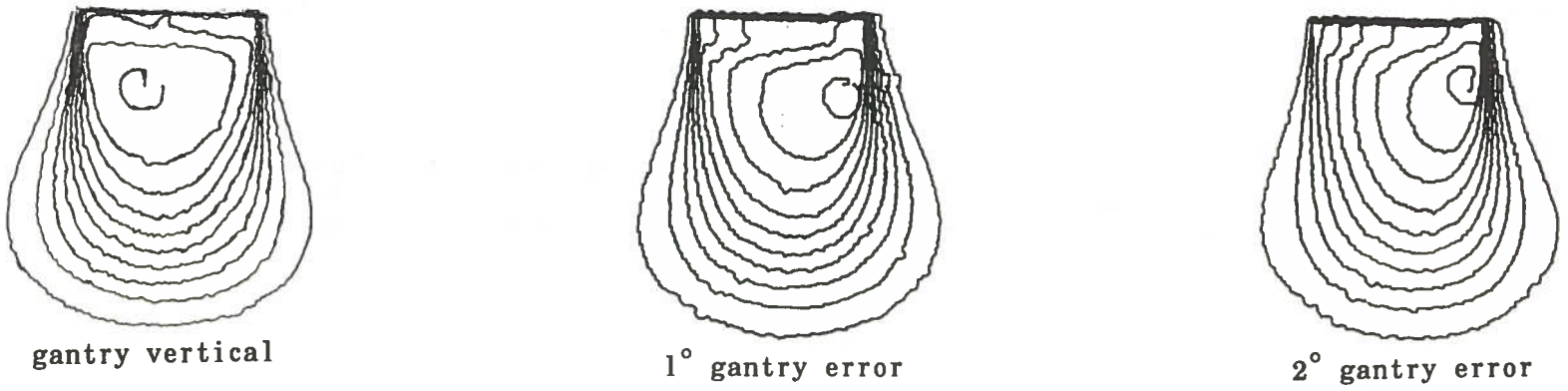

gantry vertical

1° gantry error

2° gantry error

Figure 15.3 Isodensity curves which demonstrate that the effects of angular errors depended upon cone diameter regardless of the energy of the beam.

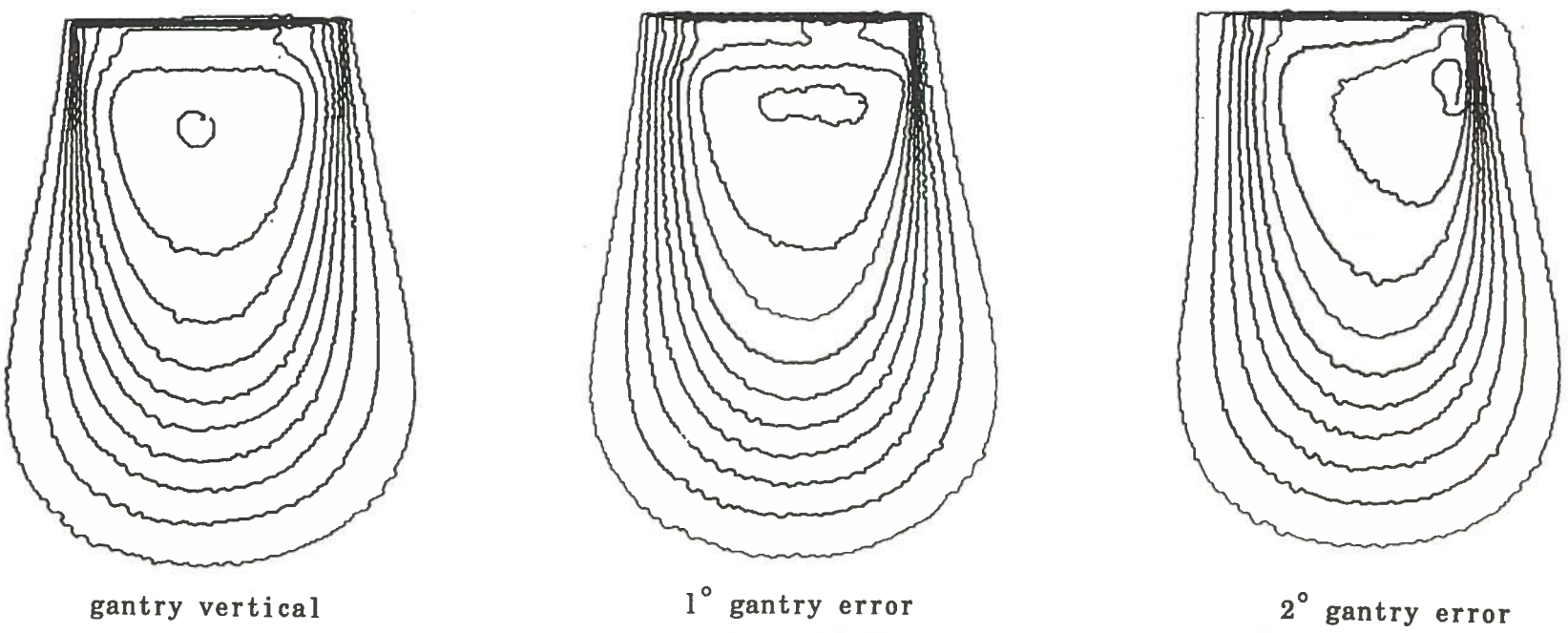

gantry vertical

1° gantry error

2° gantry error

Above: Isodensity curves generated from film irradiated with 20 MeV electrons using the 5.0 cm non-beveled cone. When the 5.0 cm cone was employed, angular errors had less of an effect than when the 3.0 cm cone was used. (Compare to 15.4.)

Figure 15.4 Isodensity curves generated from film exposed with 20 MeV electrons using the 3.0 cm non-beveled cone.

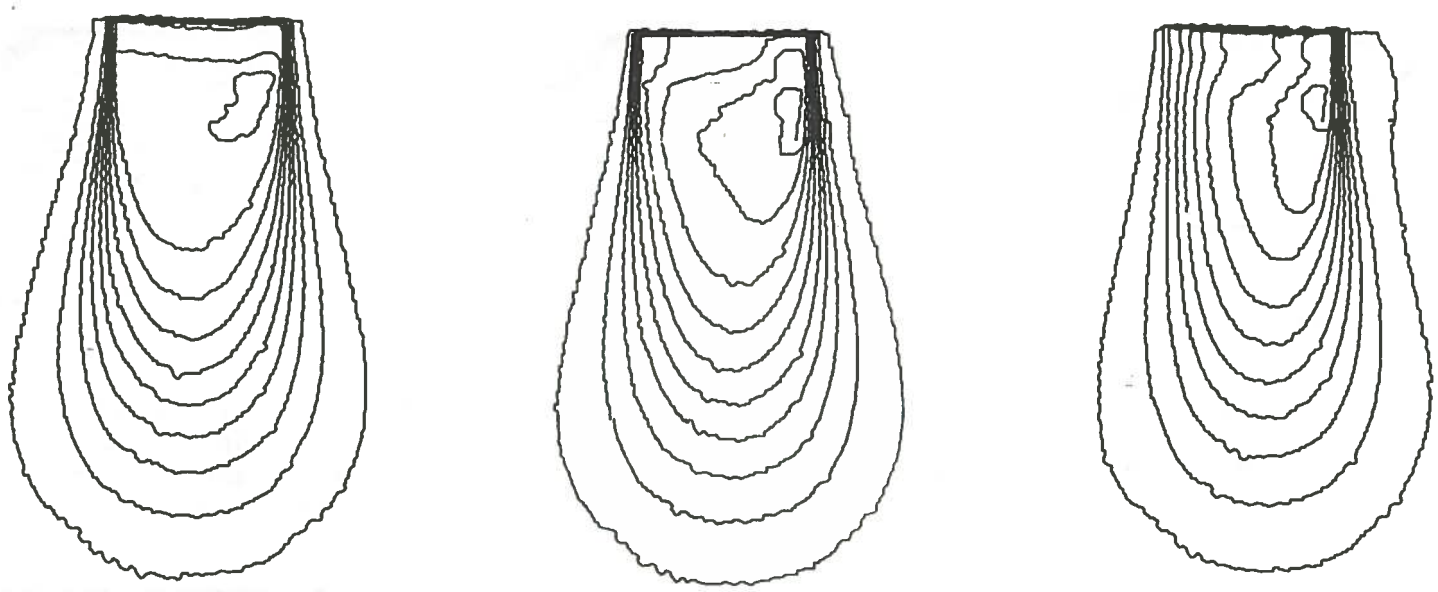

gantry vertical | 1° gantry error | 2° gantry error

Figure 16.1 The effect of angular errors was also dependent upon cone diameter for the beveled cones.

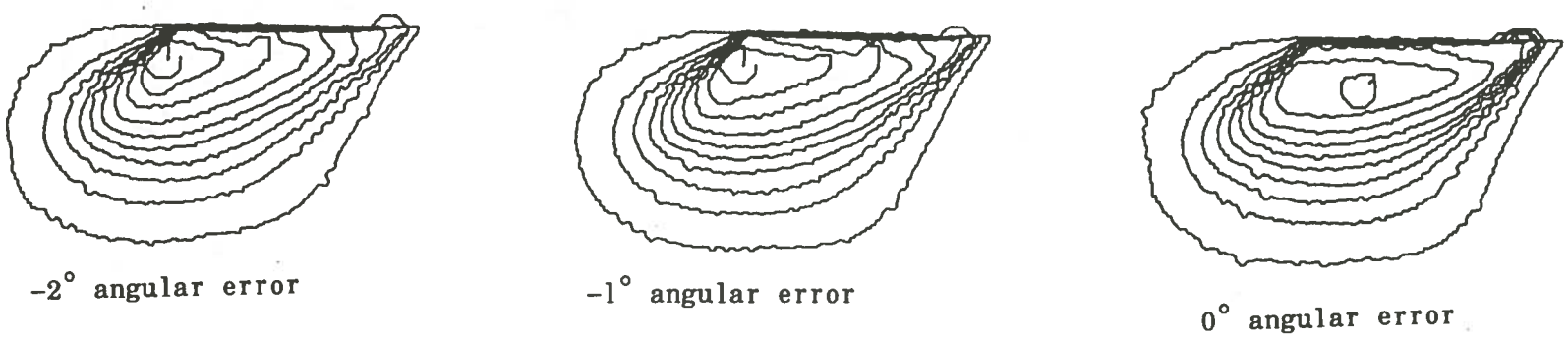

-2° angular error

-1° angular error

0° angular error

Isodensity curves generated from film exposed with 9 MeV electrons utilizing the 3.0 cm 45° beveled cone (above) and the 5.0 cm 45° beveled cone (below). Note that angular errors of minus 1 or 2 degrees had little or no effect when the larger cone was employed.

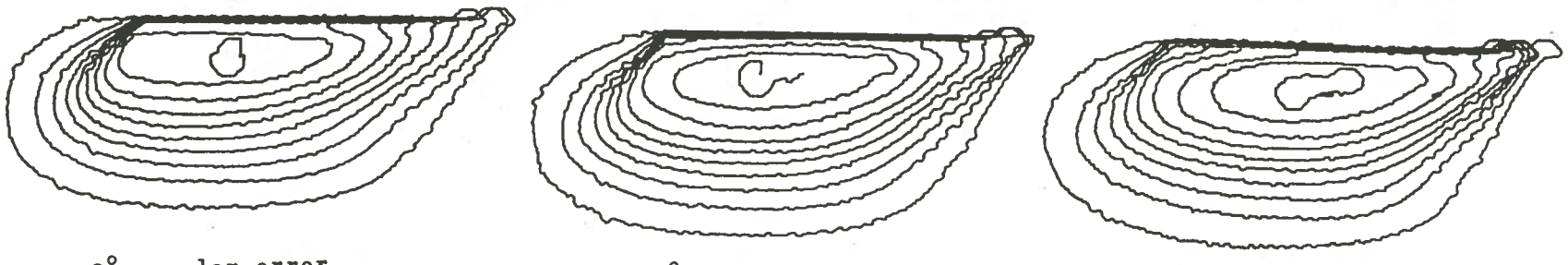

-2° angular error

-1° angular error

0° angular error

Figure 16.2 Regarding the beveled cones, angular errors in the plus direction also produced greater effects when the smaller cone was used.

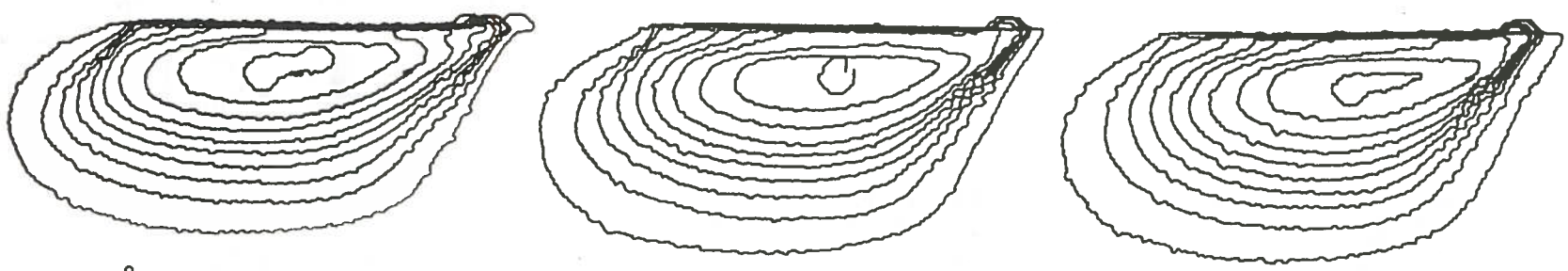

0° angular error +1° angular error +2° angular error

Isodensity curves generated from film exposed with 9 MeV electrons utilizing the 5.0 cm 45° beveled cone (above) and the 3.0 cm 45° beveled cone (below). Errors of plus 1 or 2 degrees produced little or no effect when the larger cone was employed.

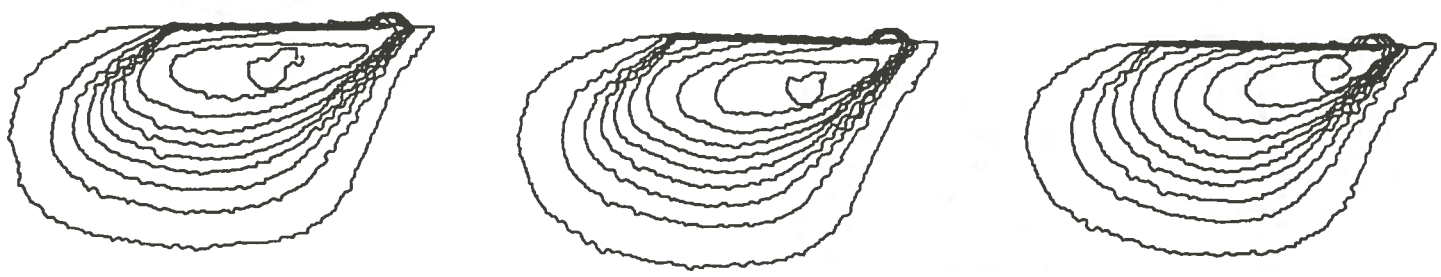

0° angular error +1° angular error +2° angular error

Figure 17. Illustrates the energy dependence of the effects.

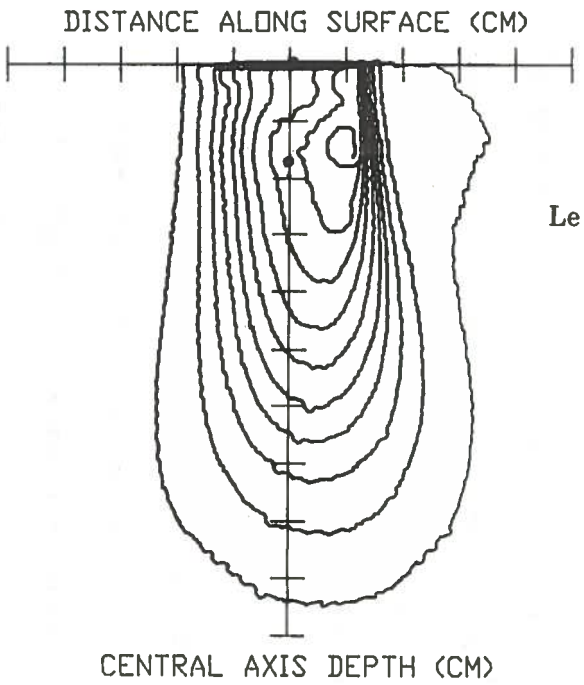

Left: With a 3° angular error, the optical density at d_{max} was greater than the 80% line when 20 MeV electrons were applied with the 3.0 cm non-beveled cone. The point on the curves designates d_{max}.

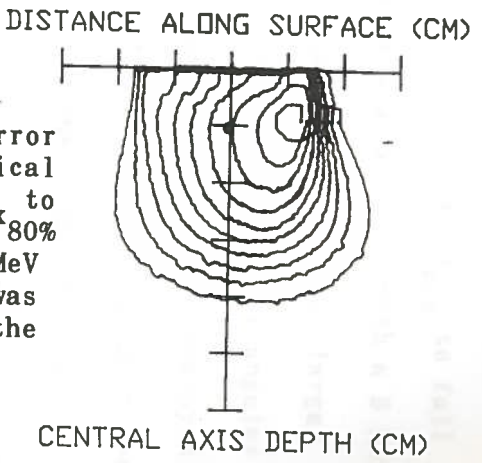

Right: A 3° angular error caused the optical density at d_{max} to fall below the 80% line when a 9 MeV electron beam was employed with the same cone.

when a 20 MeV electron beam was used with the 3.0 cm non-beveled cone. But the same gantry error caused the optical density at d_{max} to fall below the 80 percent line when the same cone was employed with a 9 MeV electron beam. But the energy dependence diminished with the larger cones (Figure 18). Figure 19 demonstrates that the effect of angular errors was also energy dependent when the beveled cones were employed.

The dose along the central axis fell off more rapidly with increased angular errors. Although this was apparent on the isodensity curves, some central axis depth-density curves are presented in Figure 20 to more accurately depict the increased falloff of dose.

With angular errors, the central axis intensity was reduced due to redirection of the original central axis, and electrons traveling parallel to it, into the distal side of the cone, therefore causing attenuation. This is represented in Figure 21 with a 5° angular error. In this diagram one can see that electrons traveling on the proximal side of the beam are directed away from the cone wall, resulting in a reduction in dose on that side of the beam axis.

The dependence upon cone diameter is analogous to the effect of field size on the significance of penumbra in a ^{60}Co beam. Just as the penumbra is more significant with small x-ray field sizes, so are the side-scattered electrons more significant with the smaller cones.

The Phantoms Compared

An electron beam is almost monoenergetic before hitting the accelerator window, but the energy is degraded as it passes through the window, the scattering foil, the monitor chamber, etc. (Khan, 1984). By the time the beam hits the phantom surface it has taken on a spectrum of

Figure 18. Isodensity curves which demonstrate that the energy dependence diminished with the larger cones.

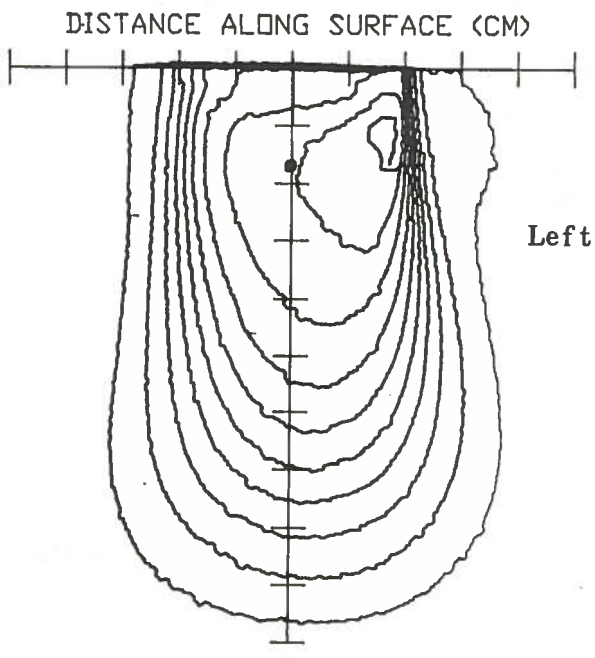

Left: With a 3° angular error the optical density at d_{max} was close to, but less than, the 90% line when 20 MeV electrons were applied with the 5.0 cm non-beveled cone.

Right: With a 3° angular error the optical density at d_{max} was also close to, but less than, the 90% line when 9 MeV electrons were applied with the same cone.

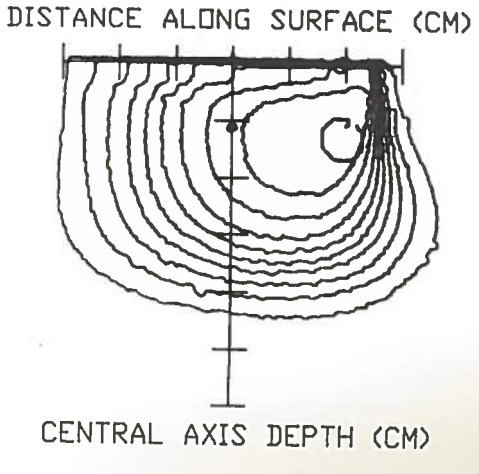

Figure 16.1 The effect of angular errors was also dependent upon cone diameter for the beveled cones.

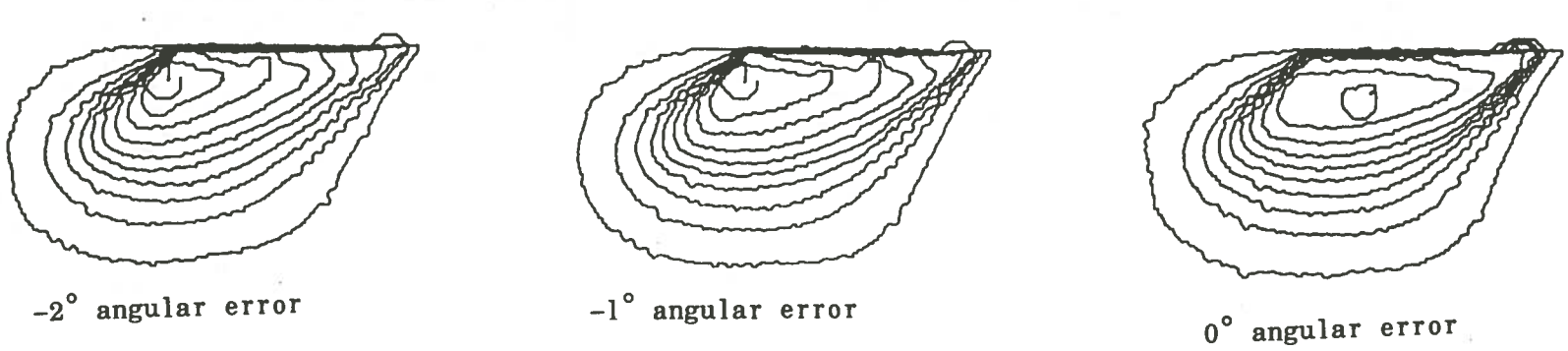

-2° angular error

-1° angular error

0° angular error

Isodensity curves generated from film exposed with 9 MeV electrons utilizing the 3.0 cm 45° beveled cone (above) and the 5.0 cm 45° beveled cone (below). Note that angular errors of minus 1 or 2 degrees had little or no effect when the larger cone was employed.

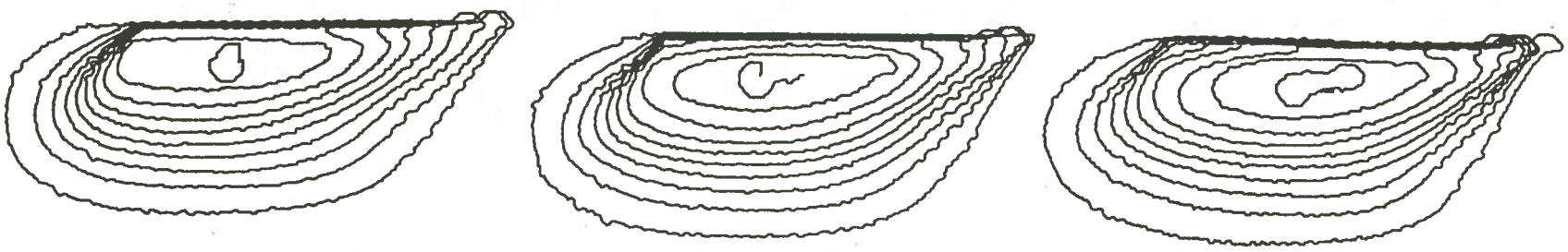

-2° angular error

-1° angular error

0° angular error

Figure 16.2 Regarding the beveled cones, angular errors in the plus direction also produced greater effects when the smaller cone was used.

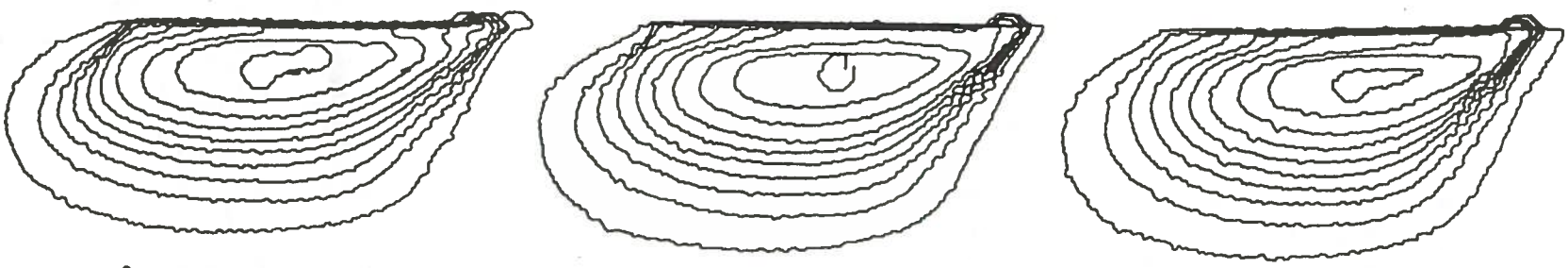

0° angular error +1° angular error +2° angular error

Isodensity curves generated from film exposed with 9 MeV electrons utilizing the 5.0 cm 45° beveled cone (above) and the 3.0 cm 45° beveled cone (below). Errors of plus 1 or 2 degrees produced little or no effect when the larger cone was employed.

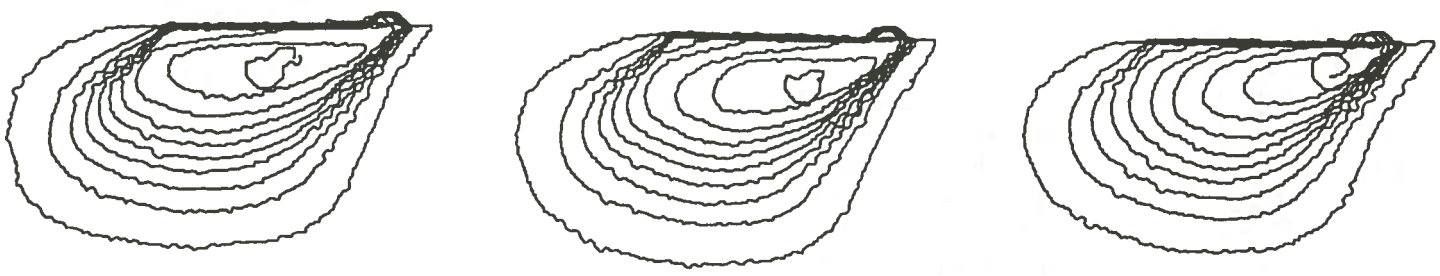

0° angular error +1° angular error +2° angular error

Figure 17. Illustrates the energy dependence of the effects.

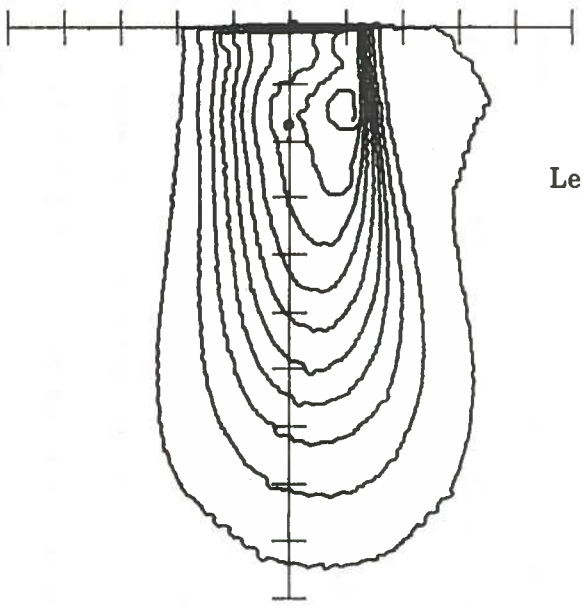

Left: With a 3° angular error, the optical density at d_{max} was greater than the 80% line when 20 MeV electrons were applied with the 3.0 cm non-beveled cone. The point on the curves designates d_{max}.

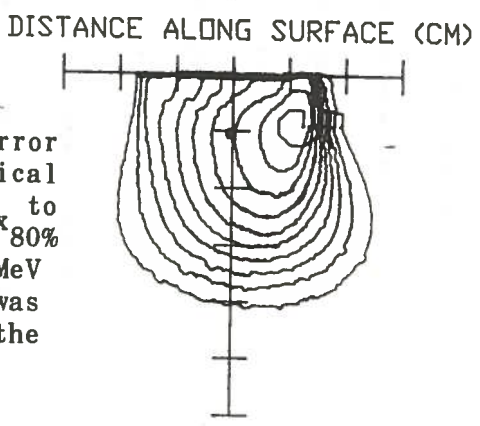

Right: A 3° angular error caused the optical density at d_{max} to fall below the 80% line when a 9 MeV electron beam was employed with the same cone.

when a 20 MeV electron beam was used with the 3.0 cm non-beveled cone. But the same gantry error caused the optical density at d_{max} to fall below the 80 percent line when the same cone was employed with a 9 MeV electron beam. But the energy dependence diminished with the larger cones (Figure 18). Figure 19 demonstrates that the effect of angular errors was also energy dependent when the beveled cones were employed.

The dose along the central axis fell off more rapidly with increased angular errors. Although this was apparent on the isodensity curves, some central axis depth-density curves are presented in Figure 20 to more accurately depict the increased falloff of dose.

With angular errors, the central axis intensity was reduced due to redirection of the original central axis, and electrons traveling parallel to it, into the distal side of the cone, therefore causing attenuation. This is represented in Figure 21 with a 5° angular error. In this diagram one can see that electrons traveling on the proximal side of the beam are directed away from the cone wall, resulting in a reduction in dose on that side of the beam axis.

The dependence upon cone diameter is analogous to the effect of field size on the significance of penumbra in a ^{60}Co beam. Just as the penumbra is more significant with small x-ray field sizes, so are the side-scattered electrons more significant with the smaller cones.

The Phantoms Compared

An electron beam is almost monoenergetic before hitting the accelerator window, but the energy is degraded as it passes through the window, the scattering foil, the monitor chamber, etc. (Khan, 1984). By the time the beam hits the phantom surface it has taken on a spectrum of

Figure 18. Isodensity curves which demonstrate that the energy dependence diminished with the larger cones.

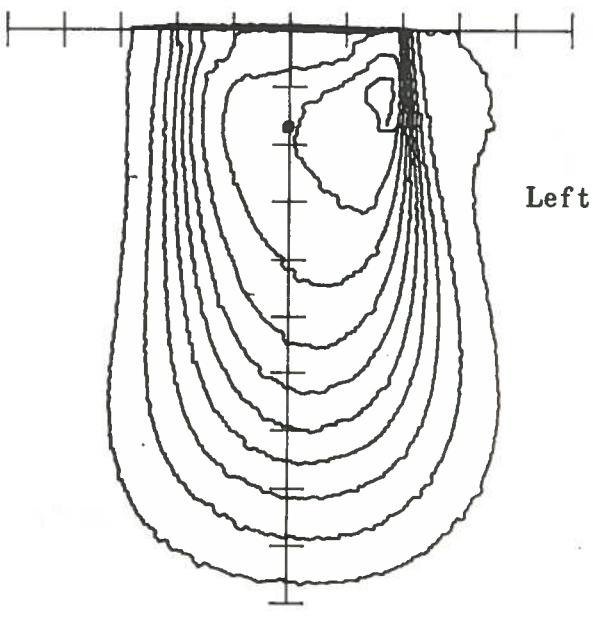

Left: With a 3° angular error the optical density at d_{max} was close to, but less than, the 90% line when 20 MeV electrons were applied with the 5.0 cm non-beveled cone.

Right: With a 3° angular error the optical density at d_{max} was also close to, but less than, the 90% line when 9 MeV electrons were applied with the same cone.

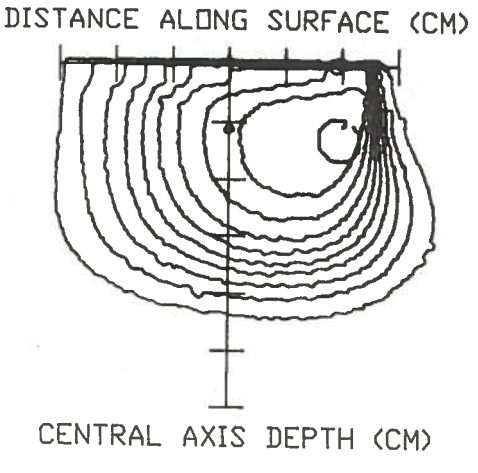

Figure 19. Isodensity curves which demonstrate that the effect was energy dependent when the beveled cones were employed.

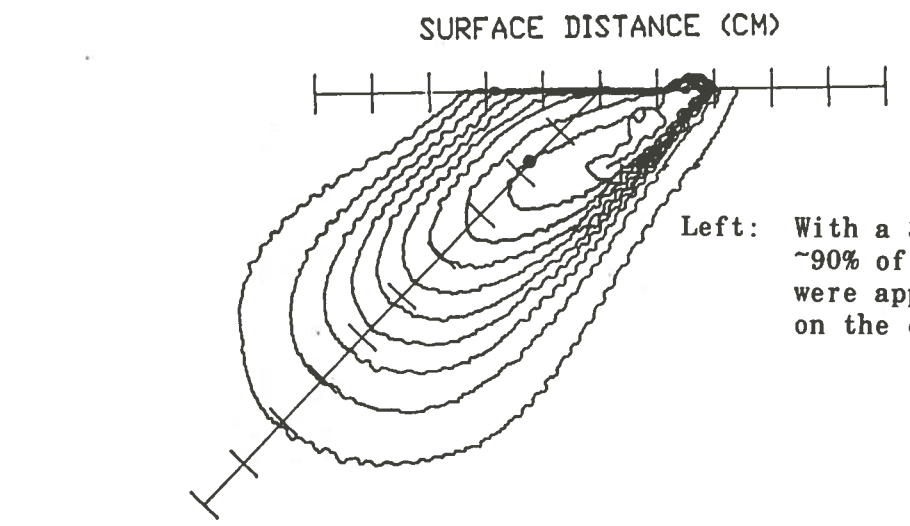

Left: With a 3° angular error, the optical density at d_{max} was ~90% of the maximum optical density when 16 MeV electrons were applied with the 3.0 cm 45° beveled cone. The point on the curves designates d_{max}.

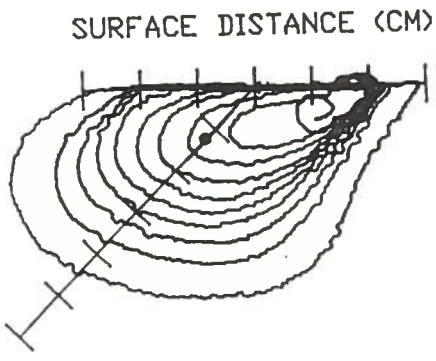

Right: A 3° angular error caused the optical density at d_{max} to fall well below the 90% line when a 9 MeV beam was employed with the same cone.

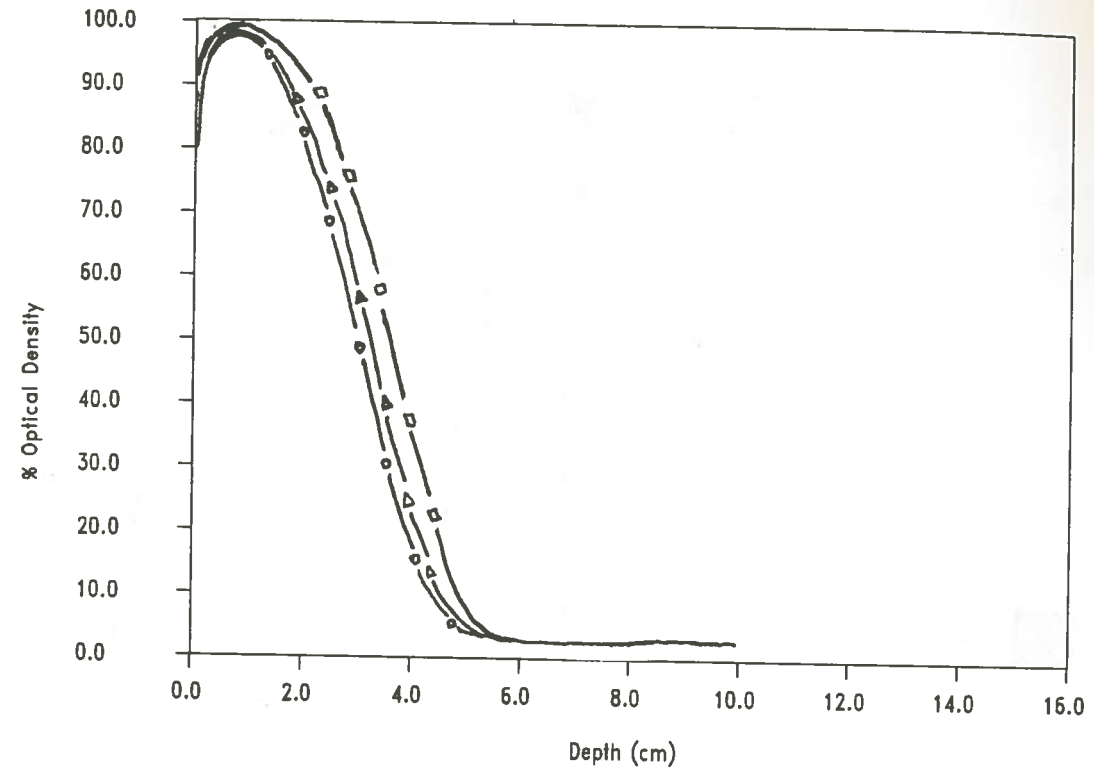

□ gantry vertical

Δ 3° angular error

O 5° angular error

Figure 20. Central axis depth-density curves generated from film irradiated with 9 MeV electrons using the 5.0 cm non-beveled cone. Depicts an increased falloff in dose with increased angular errors.